International Journal of Solids and Structures 000 (2016) 1–17

Contents lists available at ScienceDirect

International Journal of Solids and Structures

journal homepage: www.elsevier.com/locate/ijsolstr

On buckling of a soft incompressible electroactive hollow cylinder

Yipin Su[a,b], Weijian Zhou[a,b], Weiqiu Chen[a,b,c,d], Chaofeng Lü[c,d,e,*]

[a] Department of Engineering Mechanics, Zhejiang University, Hangzhou 310027, PR China
[b] State Key Laboratory of Fluid Power and Mechatronic Systems, Zhejiang University, Hangzhou 310027, PR China
[c] Key Laboratory of Soft Machines and Smart Devices of Zhejiang Province, Zhejiang University, Hangzhou 310027, PR China
[d] Soft Matter Research Center, Zhejiang University, Hangzhou 310027, PR China
[e] Department of Civil Engineering, Zhejiang University, Hangzhou 310058, PR China

ARTICLE INFO

Article history:
Received 11 April 2016
Revised 5 June 2016
Available online xxx

Keywords:
Soft electroactive materials
Hollow cylinder
Nonlinear buckling
Linear incremental theory
Finite deformation

ABSTRACT

Soft electroactive materials show great potential for device and robot applications. However, these materials are apt to experience buckling and pull-in instability under critical pressure or voltage, and, therefore, their practical applications are more or less prevented. In this paper, buckling behavior of incompressible soft electroactive hollow cylinders is investigated based on the nonlinear theory of electroelasticity and the associated linear incremental field theory. Hollow cylinders including or excluding the effects of exterior electric field are studied in a comparison manner. The equations governing the linearized incremental motion upon a finitely deformed configuration in the presence of an electric field are derived and exactly solved by introducing three displacement functions. As an illustrative example, the generic isotropic electroactive materials are considered and results are presented for a simple model of ideal electroelastic material. Numerical calculations show that the buckling of electroactive hollow cylinders is significantly influenced by the biasing fields, the electromechanical coupling parameters, the geometrical parameters of the cylinder, and the electric field outside the cylinder. In particular, a phase diagram is constructed based on the numerical results to clearly identify the dominant buckling modes and the transition between them in the $\kappa - -\nu$ (axial wave number versus radius ratio) plane.

1. Introduction

Commonly, the instability phenomenon is considered as negative that should be accurately predicted and carefully avoided. Stabilities of elastic bodies have attracted considerable attention since Euler's classical work on the buckling of thin columns (Euler and Carathéodory, 1952). It is well known that a slender elastic body will buckle under a sufficiently large compressive load, the so-called Euler buckling.

Wilkes (1955) seems to be the first to address the instability of a cylindrical shell under axial load by using three-dimensional theory of nonlinear elasticity. The linearized system around a finite axial strain was solved exactly in terms of Bessel functions. It was found that the bifurcation curves for the incompressible neo-Hookean material have a horizontal asymptote of $\lambda \approx 0.444$, which corresponds to surface instability of a compressed half-space. However, Wilkes's calculation was confined to the axisymmetric mode ($n = 0$). Pan and Beatty (1997) considered an incompressible cylindrical tube and derived the formulation of bifurcation criterion including both axisymmetric mode ($n = 0$) and asymmetric mode ($n = 1$). They compared the results obtained using neo-Hookean, Mooney–Rivlin and Gent–Thomas models. Dorfmann and Haughton (2006) extended the theory to look at a selection of compressible materials and considered higher order bifurcation modes. It was shown that long thick-walled tube undergoes asymmetric mode buckling while short thick-walled tube undergoes axisymmetric mode buckling at some critical loading. However, for thin-walled tube, the occurrence of various critical bifurcation modes ($n = 0, 1, 2, 3, \ldots$) depends on the length of the tube. Goriely et al. (2008) used the Stroh formalism to investigate the instability of an incompressible cylindrical shell under axial load, and expanded the exact solution up to order 2, 4 and 6 so as to make a comparative study.

Soft electroactive materials have appeared as smart materials which enable realizing the conversion between electrical and mechanical energies. Due to their low weight, rapid response and large deformation under electrical stimulus, soft electroactive materials are widely used to develop high-performance devices such as actuators, artificial muscles, energy harvesters and space robotics (Pelrine et al., 2000; Bhattacharya et al., 2004; O'Halloran et al., 2008). The strong nonlinearity and the electrome-

* Corresponding author at: Department of Civil Engineering, Zhejiang University, Hangzhou 310058, PR China.
E-mail address: lucf@zju.edu.cn (C. Lü).

http://dx.doi.org/10.1016/j.ijsolstr.2016.07.008
0020-7683/

chanical coupling should be taken into account in the analysis of soft electroactive materials or structures. The formulation of a general nonlinear theory of electroelasticity was first developed by Toupin (1956) and has been intensively studied in recent years (McMeeking and Landis, 2005; Dorfmann and Ogden, 2006; Ericksen, 2007; Suo et al., 2008; Ogden, 2009).

Electroactive materials are often working under extremely high voltage, thus susceptible to fail in the form of electromechanical instability which can be a precursor of electrical breakdown (Stark and Garton, 1955; Blok and LeGrand, 1969). Such instability phenomenon poses a clear limitation in the development of devices based on electroactive materials. Careful modeling and analyses are therefore required.

Experiments showed the coexistence of two regions, i.e., flat and wrinkles, in an electroactive film when subjected to critical applied voltage. Stable wrinkles arise first and then pull-in instability occurs as the applied voltage keeps increasing (Plante and Dubowsky, 2006). Zhao et al. (2007) and Zhao and Suo (2007) demonstrated that the electroactive film will undergo inhomogeneous deformation because the free-energy function of the elastomer is typically nonconvex, and that the electromechanical instability occurs when the generalized tangent modulus ceases to be positive definite. They further revealed that the electromechanical instability of electroactive materials can be considerably enhanced by prestress. Dorfmann and Ogden (2010) considered the stability of an incompressible electroactive half-space subjected to pure homogeneous compression in the presence of an applied electric field normal to its surface. They (Dorfmann and Ogden, 2014) also investigated the instability of an equibiaxially stretched electroelastic plate with and without the effects of exterior electric field, which exhibits different features because of the differences in electric boundary conditions. Díaz-Calleja et al. (2009) analyzed the bifurcation characteristics of two biaxially stretched incompressible rubber slabs, one with flexible electrodes on its two surfaces, and the other floating between two fixed electrodes. It was shown that the effects of electric field on the bifurcation of the two slabs are inverse and the pull-in phenomenon in the second case can be prevented if the gap between the sample and the electrodes is large enough. Recently, dielectric composites have attracted considerable interests because they can markedly improve the performance of dielectric devices (Huang et al., 2004; deBotton et al., 2007). The stability of multilayered soft dielectrics were systematically investigated by Bertoldi and Gei (2011) and Rudykh and deBotton (2011).

Dielectric elastomer tube actuator (DETA) was proposed first by Pelrine et al. (1998). Compared to other dielectric elastomer configurations (for example, plate and membrane actuators), DETA has very low inactive-to-active material ratio, and is less bulky but more versatile for applications (Carpi and Rossi, 2004; Cameron et al., 2008). Similarly, DETA is also susceptible to electromechanical instability. Thus, it is necessary to analyze the stability of electroactive material of cylindrical structure. Zhu et al. (2010) obtained an analytical solution for the finite deformation of a DETA which is mechanically prestretched and actuated by a voltage. They also studied the effects of prestretch and geometry on electromechanical instabilities of the tube actuator using a linear perturbation method. Zhou et al. (2014) demonstrated that the electromechanical instability of a DETA could be avoided, and larger actuation deformation may be achieved by applying specific boundary constraints. Most recently, Zhang et al. (2015) examined four failure modes of a DETA, including loss of tension, electrical breakdown, snap-through instability and tensile rupture.

The so-called Hessian approach was widely adopted to analyze the stability of electroactive material (Zhao et al., 2007; Zhao and Suo 2007; Díaz-Calleja et al., 2009). However, these analyses were only limited to homogeneous deformations, and the associate results did not reflect the dependence of buckling behavior on the geometry of the structure. Taking both geometry and non-homogeneous deformation into consideration, the occurrence of diffuse modes of an electroactive hollow cylinder subjected to a uniform biasing electric field is exactly investigated in this paper. The governing equations will be derived in form of incremental fields upon a finite deformation state. By introducing three displacement functions, exact solutions are presented in terms of Bessel functions, and, with the incorporation of boundary conditions, the characteristic equation for buckling behavior of the cylinder is derived. A simple prototype model, namely the neo-Hookean electroelastic material, is considered as an illustrative example. A simple scaling law involving the normalized critical compression and normalized wave number is derived for tuning the buckling behavior of the cylinder. Numerical calculations will be performed to examine the effects of material parameters, biasing electric field, and geometrical configuration on the buckling properties of the cylinder. The influence of the electric field in the vacuum exterior to the cylinder will also be investigated through comparative studies.

2. Finite deformation and incremental motion

For better understanding the derivations, the general formulations associated with the nonlinear electroelasticity and the linear incremental field theory (Dorfmann and Ogden, 2006; Ogden, 2009) are briefly reviewed in Appendix A. Consider an isotropic, incompressible soft electroactive hollow cylinder with initial length L, inner radius R_i, and outer radius R_o, respectively. The radius ratio of the cylindrical shell is denoted by $\nu = R_i/R_o$. The cylinder is assumed subjected to an axial mechanical load and a uniaxial biasing electric displacement D_z that is aligned with the axial direction. The hollow cylinder then deforms to become a one with length l, and inner and outer radii r_i and r_o, respectively. The initial and current cylindrical coordinates are respectively designated as (R, Θ, Z) and (r, θ, z) with the origin located at the center of one end of the cylinder. For incompressible materials, the principal stretches of the cylinder are

$$\lambda_z = \lambda, \quad \lambda_r = \lambda_\theta = \lambda^{-1/2} \tag{1}$$

Then, the deformation gradient $\mathbf{F}$ is given by

$$\mathbf{F} = \begin{bmatrix} \lambda^{-1/2} & 0 & 0 \\ 0 & \lambda^{-1/2} & 0 \\ 0 & 0 & \lambda \end{bmatrix}. \tag{2}$$

For axisymmetric deformation, the non-zero components of the total stress tensor and electric field vector may be derived from Eq. (A1) as (Dorfmann and Ogden, 2006; Ogden, 2009; Chen and Dai, 2012):

$$\tau_{rr} = \tau_{\theta\theta} = 2W_1\lambda^{-1} + 2W_2\left(I_1\lambda^{-1} - \lambda^{-2}\right) - p, \tag{3a}$$

$$\tau_{zz} = 2W_1\lambda^2 + 2W_2\left(I_1\lambda^2 - \lambda^4\right) + 2W_5D_z^2 + 4W_6\lambda^2D_z^2 - p, \tag{3b}$$

$$E_z = 2\left(W_4\lambda^{-2} + W_5 + W_6\lambda^2\right)D_z, \tag{3c}$$

where $W_m = \partial W/\partial I_m$, with I_m being the mth invariant as given in Eq. (A2). It is straightforward from Eq. (3c) that

$$D_z = \frac{E_z}{2\left(W_4\lambda^{-2} + W_5 + W_6\lambda^2\right)} = \varepsilon E_z, \tag{4}$$

which implies that the permittivity of the material relies on the deformation of the cylinder, i.e., $\varepsilon = \varepsilon(\lambda)$, if $W_4 \neq 0$ or $W_6 \neq 0$.

Considering the effects of exterior electric fields ($r < r_i$ or $r > r_o$), the boundary conditions in the second and third equa-

tions of (A4) at $r = r_i$ and $r = r_o$ read as $(\mathbf{E} - \mathbf{E}^*_m) \times \mathbf{n}_m = \mathbf{0}$ and $(\mathbf{D} - \mathbf{D}^*_m) \cdot \mathbf{n}_m = 0 (m = o, i)$ respectively, where $n_o = (1, 0, 0)$ and $n_i = (-1, 0, 0)$. Combining them with Eq. (3), we have

$$E^*_{oz} = E^*_{iz} = E_z = \frac{D_z}{\varepsilon},$$
$$D^*_{oz} = D^*_{iz} = \frac{\varepsilon_0}{\varepsilon} D_z,$$
$$\tau^*_{orr} = \tau^*_{o\theta\theta} = -\tau^*_{ozz} = \tau^*_{irr} = \tau^*_{i\theta\theta} = -\tau^*_{izz} = -\frac{\varepsilon_0}{2\varepsilon^2} D_z^2, \tag{5}$$

where and in the text hereafter the superscript star represents the corresponding physical quantities in vacuum, while ε_0 is the permittivity of vacuum.

It is apparent that the stress and electric fields in the hollow cylinder and/or exterior vacuum space are all uniform. Without the action of applied mechanical traction on the two lateral cylindrical surfaces, the *hydrostatic pressure* p may be determined by the relation $\tau_{rr} = \tau^*_{orr} = \tau^*_{irr}$ as

$$p = 2W_1 \lambda^{-1} + 2W_2 \left(I_1 \lambda^{-1} - \lambda^{-2}\right) + \frac{\varepsilon_0}{2\varepsilon^2} D_z^2. \tag{6}$$

Substituting Eq. (6) into Eq. (3b), τ_{zz} may be completely determined which should meet the mechanical boundary conditions at the ends.

Now, consider a small increment superimposed on the deformed configuration of the hollow cylinder. With the underlying deformed state as the reference configuration, the incremental displacement components may be expressed as $u_i = u_i(r, \theta, z)$ $(i = r, \theta, z)$. The displacement gradient is obtained as

$$\mathbf{H} = \begin{bmatrix} \frac{\partial u_r}{\partial r} & \frac{1}{r}\left(\frac{\partial u_r}{\partial \theta} - u_\theta\right) & \frac{\partial u_r}{\partial z} \\ \frac{\partial u_\theta}{\partial r} & \frac{1}{r}\left(\frac{\partial u_\theta}{\partial \theta} + u_r\right) & \frac{\partial u_\theta}{\partial z} \\ \frac{\partial u_z}{\partial r} & \frac{1}{r}\frac{\partial u_z}{\partial \theta} & \frac{\partial u_z}{\partial z} \end{bmatrix} \tag{7}$$

The incompressibility condition in Eq. (A8) becomes

$$\frac{\partial u_r}{\partial r} + \frac{1}{r}\left(\frac{\partial u_\theta}{\partial \theta} + u_r\right) + \frac{\partial u_z}{\partial z} = 0. \tag{8}$$

In general, the electric field is irrotational which allows the incremental electric field to be expressed as

$$\dot{E}_{l0r} = -\frac{\partial \phi}{\partial r}, \quad \dot{E}_{l0\theta} = -\frac{1}{r}\frac{\partial \phi}{\partial \theta}, \quad \dot{E}_{l0z} = -\frac{\partial \phi}{\partial z}, \tag{9}$$

where ϕ is the electric potential in the cylinder.

According to the linear incremental field theory (Dorfmann and Ogden, 2006; Ogden, 2009), substitution of Eqs. (7) and (9) into Eq. (A6) gives rise to the components of the incremental stress and electric fields as

$$\dot{D}_{l0r} = e_{15}\left(\frac{\partial u_r}{\partial z} + \frac{\partial u_z}{\partial r}\right) - \varepsilon_{11}\frac{\partial \phi}{\partial r},$$
$$\dot{D}_{l0\theta} = e_{15}\left(\frac{\partial u_\theta}{\partial z} + \frac{1}{r}\frac{\partial u_z}{\partial \theta}\right) - \varepsilon_{11}\frac{1}{r}\frac{\partial \phi}{\partial \theta},$$
$$\dot{D}_{l0z} = e_{31}\left[\frac{\partial u_r}{\partial r} + \frac{1}{r}\left(\frac{\partial u_\theta}{\partial \theta} + u_r\right)\right] + e_{33}\frac{\partial u_z}{\partial z} - \varepsilon_{33}\frac{\partial \phi}{\partial z},$$
$$\dot{T}_{0rr} = (c_{11} + p)\frac{\partial u_r}{\partial r} + c_{12}\frac{1}{r}\left(\frac{\partial u_\theta}{\partial \theta} + u_r\right) + c_{13}\frac{\partial u_z}{\partial z} + e_{31}\frac{\partial \phi}{\partial z} - \dot{p},$$
$$\dot{T}_{0\theta\theta} = c_{12}\frac{\partial u_r}{\partial r} + (c_{11} + p)\frac{1}{r}\left(\frac{\partial u_\theta}{\partial \theta} + u_r\right) + c_{13}\frac{\partial u_z}{\partial z} + e_{31}\frac{\partial \phi}{\partial z} - \dot{p},$$
$$\dot{T}_{0zz} = c_{13}\frac{\partial u_r}{\partial r} + c_{13}\frac{1}{r}\left(\frac{\partial u_\theta}{\partial \theta} + u_r\right) + (c_{33} + p)\frac{\partial u_z}{\partial z} + e_{33}\frac{\partial \phi}{\partial z} - \dot{p},$$
$$\dot{T}_{0r\theta} = c_{661}\frac{\partial u_\theta}{\partial r} + (c_{662} + p)\frac{1}{r}\left(\frac{\partial u_r}{\partial \theta} - u_\theta\right),$$
$$\dot{T}_{0\theta r} = c_{661}\frac{1}{r}\left(\frac{\partial u_r}{\partial \theta} - u_\theta\right) + (c_{662} + p)\frac{\partial u_\theta}{\partial r},$$
$$\dot{T}_{0rz} = (c_{551} + p)\frac{\partial u_r}{\partial z} + c_{552}\frac{\partial u_z}{\partial r} + e_{15}\frac{\partial \phi}{\partial r},$$
$$\dot{T}_{0zr} = c_{553}\frac{\partial u_r}{\partial z} + (c_{551} + p)\frac{\partial u_z}{\partial r} + e_{15}\frac{\partial \phi}{\partial r},$$
$$\dot{T}_{0\theta z} = c_{552}\frac{1}{r}\frac{\partial u_z}{\partial \theta} + (c_{551} + p)\frac{\partial u_\theta}{\partial z} + e_{15}\frac{1}{r}\frac{\partial \phi}{\partial \theta},$$
$$\dot{T}_{0z\theta} = c_{553}\frac{\partial u_\theta}{\partial z} + (c_{551} + p)\frac{1}{r}\frac{\partial u_z}{\partial \theta} + e_{15}\frac{1}{r}\frac{\partial \phi}{\partial \theta}, \tag{10}$$

where c_{ij} (or c_{ijk}), e_{ij}, and ε_{ij} are the effective electroelastic moduli of the cylinder under the action of initial biasing electric displacement D_z and pre-stretch λ. They are related to the deformation gradient $\mathbf{F}$ and D_z according to Eq. (A7). The detailed formulations may be referred to Su et al. (2016) and not reproduced here for compact.

Substituting Eq. (10) into the differential equations of motion $(A9)_{1,\,3}$, we obtain

$$\left[e_{15}\nabla^2 + (e_{33} - e_{31} - e_{15})\frac{\partial^2}{\partial z^2}\right]u_z - \left(\varepsilon_{11}\nabla^2 + \varepsilon_{33}\frac{\partial^2}{\partial z^2}\right)\phi = 0$$
$$\left[c_{11}\left(\frac{\partial^2}{\partial r^2} + \frac{1}{r}\frac{\partial}{\partial r} - \frac{1}{r^2}\right) + c_{661}\frac{1}{r^2}\frac{\partial^2}{\partial \theta^2} + c_{553}\frac{\partial^2}{\partial z^2}\right]u_r$$
$$+\left[(c_{662} + c_{12})\frac{1}{r}\frac{\partial^2}{\partial r \partial \theta} - (c_{11} + c_{661})\frac{1}{r^2}\frac{\partial}{\partial \theta}\right]u_\theta$$
$$+(c_{13} + c_{551})\frac{\partial^2 u_z}{\partial r \partial z} + (e_{31} + e_{15})\frac{\partial^2 \phi}{\partial r \partial z} - \frac{\partial \dot{p}}{\partial r} = 0,$$
$$\left[(c_{662} + c_{12})\frac{1}{r}\frac{\partial^2}{\partial r \partial \theta} + (c_{11} + c_{661})\frac{1}{r^2}\frac{\partial}{\partial \theta}\right]u_r$$
$$+\left[c_{661}\left(\frac{\partial^2}{\partial r^2} + \frac{1}{r}\frac{\partial}{\partial r} - \frac{1}{r^2}\right) + c_{11}\frac{1}{r^2}\frac{\partial^2}{\partial \theta^2} + c_{553}\frac{\partial^2}{\partial z^2}\right]u_\theta$$
$$+(c_{13} + c_{551})\frac{1}{r}\frac{\partial^2 u_z}{\partial \theta \partial z} + (e_{31} + e_{15})\frac{1}{r}\frac{\partial^2 \phi}{\partial \theta \partial z} - \frac{1}{r}\frac{\partial \dot{p}}{\partial \theta} = 0,$$
$$(c_{551} + c_{13})\left(\frac{\partial^2}{\partial r \partial z} + \frac{1}{r}\frac{\partial}{\partial z}\right)u_r + (c_{13} + c_{551})\frac{1}{r}\frac{\partial^2 u_\theta}{\partial \theta \partial z}$$
$$+\left(c_{552}\nabla^2 + c_{33}\frac{\partial^2}{\partial z^2}\right)u_z + \left(e_{15}\nabla^2 + e_{33}\frac{\partial^2}{\partial z^2}\right)\phi - \frac{\partial \dot{p}}{\partial z} = 0, \tag{11}$$

where $\nabla^2 = \frac{\partial^2}{\partial r^2} + \frac{1}{r}\frac{\partial}{\partial r} + \frac{1}{r^2}\frac{\partial^2}{\partial \theta^2}$ is the two-dimensional Laplace operator.

Assuming that the cylinder is under end thrust with the two end cross-sections remaining plane and the two lateral cylindrical surfaces are traction-free. The boundary conditions for the incremental fields may be expressed as

$$\dot{E}_{l0\theta} - \dot{E}^*_{m\theta} - E^*_{mz}\frac{1}{r}\frac{\partial u_z}{\partial \theta} = 0, \quad \dot{E}_{l0z} - \dot{E}^*_{mz} - E^*_{mz}\frac{\partial u_z}{\partial z} = 0,$$
$$\dot{D}_{l0r} + D^*_{mz}\frac{\partial u_r}{\partial z} - \dot{D}^*_{mr} = 0 \quad (r = r_m; \;\; m = o, i), \tag{12}$$

$$\dot{T}_{0rr} = \dot{\tau}^*_{mrr} - \tau^*_{mrr}\frac{\partial u_r}{\partial r}, \; \dot{T}_{0r\theta} = \dot{\tau}^*_{m\theta r} - \tau^*_{m\theta\theta}\frac{1}{r}\left(\frac{\partial u_r}{\partial \theta} - u_\theta\right),$$
$$\dot{T}_{0rz} = \dot{\tau}^*_{mzr} - \tau^*_{mzz}\frac{\partial u_r}{\partial z} \; (r = r_m; \;\; m = o, i), \tag{13}$$

Please cite this article as: Y. Su et al., On buckling of a soft incompressible electroactive hollow cylinder, International Journal of Solids and Structures (2016), http://dx.doi.org/10.1016/j.ijsolstr.2016.07.008

where the non-zero components of the incremental Maxwell stress $\dot{\tau}^*_{mij}$ are derived from Eq. (A13) as

$$\dot{\tau}^*_{mrr} = \dot{\tau}^*_{m\theta\theta} = -\dot{\tau}^*_{mzz} = -\varepsilon_0 E^*_z \dot{E}^*_z,$$
$$\dot{\tau}^*_{mrz} = \dot{\tau}^*_{mzr} = \varepsilon_0 E^*_z \dot{E}^*_r, \quad \dot{\tau}^*_{m\theta r} = 0 (m = o, i), \tag{14}$$

while the incremental electric displacement and electric field in the vacuum space satisfy $\dot{D}^*_{mj} = \varepsilon_0 \dot{E}^*_{mj}$ with $\dot{E}^*_{mj}$, from the nature of irrotational electric field, expressed by

$$\dot{E}^*_{mr} = -\frac{\partial \dot{\phi}^*_m}{\partial r}, \quad \dot{E}^*_{m\theta} = -\frac{1}{r}\frac{\partial \dot{\phi}^*_m}{\partial \theta}, \quad \dot{E}^*_{mz} = -\frac{\partial \dot{\phi}^*_m}{\partial z}. \tag{15}$$

where $\dot{\phi}^*_m$ is the electric potential in vacuum. Combining Eq. (15) with Eq. (A12) makes the following Laplace's equation hold for $\dot{\phi}^*_m$

$$\nabla^2 \dot{\phi}^*_m + \frac{\partial^2 \dot{\phi}^*_m}{\partial z^2} = 0 \quad (m = o, i). \tag{16}$$

Eqs. (12)–(16) indicate that the boundary conditions for a soft electroactive cylinder in incremental motion depend on the exterior electric field that is governed by Eq. (16).

3. Buckling analysis

Eqs. (8) and (11) govern the incremental motion upon finite deformation of the electroactive hollow cylinder in terms of five unknown functions $u_r, u_\theta, u_z, \phi, \dot{p}$. Similar to the treatment for infinitesimal motion of a transversely isotropic body (Ding and Chen, 2001; Ding et al., 2006; Su et al., 2016), we introduce three displacement functions ψ, G, and U in the manner of

$$u_r = \frac{1}{r}\frac{\partial \psi}{\partial \theta} - \frac{\partial G}{\partial r}, \quad u_\theta = -\frac{\partial \psi}{\partial r} - \frac{1}{r}\frac{\partial G}{\partial \theta}, \quad u_z = U. \tag{17}$$

Then Eqs. (8) and (11) are reduced to

$$\left(c_{661}\nabla^2 + c_{553}\frac{\partial^2}{\partial z^2}\right)\psi = 0,$$
$$\left[(c_{11} - c_{13} - c_{551})\nabla^2 + c_{553}\frac{\partial^2}{\partial z^2}\right]G - (e_{31} + e_{15})\frac{\partial \phi}{\partial z} + \dot{p} = 0,$$
$$\left[c_{552}\nabla^2 + (c_{33} - c_{13} - c_{551})\frac{\partial^2}{\partial z^2}\right]U + \left(e_{15}\nabla^2 + e_{33}\frac{\partial^2}{\partial z^2}\right)\phi - \frac{\partial \dot{p}}{\partial z} = 0,$$
$$\left[e_{15}\nabla^2 + (e_{33} - e_{31} - e_{15})\frac{\partial^2}{\partial z^2}\right]U - \left(\varepsilon_{11}\nabla^2 + \varepsilon_{33}\frac{\partial^2}{\partial z^2}\right)\phi = 0,$$
$$-\nabla^2 G + \frac{\partial U}{\partial z} = 0, \tag{18}$$

where the relation $c_{11} - c_{12} - c_{662} = c_{661}$ has been used. Note that the displacement function ψ is decoupled from the other four unknown functions, which makes the equation system much simpler.

Buckling of the cylinder requires a non-trivial solution to the linearized equations of small incremental deformation. For the incremental motion of the cylinder, we consider the slippage effects at the two ends described by the following boundary conditions:

$$U(r, \theta, 0) = U(r, \theta, l) = 0, \tag{19a}$$

$$\dot{T}_{0z\theta}(r, \theta, 0) = \dot{T}_{0z\theta}(r, \theta, l) = 0, \tag{19b}$$

$$\dot{T}_{0zr}(r, \theta, 0) = \dot{T}_{0zr}(r, \theta, l) = 0. \tag{19c}$$

Then the solution for the linear equations of incremental field may be assumed in the form

$$\begin{Bmatrix} \psi \\ G \\ \dot{p} \end{Bmatrix} = \sum_{n=1}^{\infty}\sum_{q=0}^{\infty} \begin{Bmatrix} \bar{\psi}_n(r)\sin(n\theta) \\ \bar{G}_n(r)\cos(n\theta) \\ \bar{\dot{p}}_n(r)\cos(n\theta) \end{Bmatrix} \cos\left(\tfrac{q\pi z}{\lambda L}\right),$$
$$\begin{Bmatrix} U \\ \phi \\ \phi^*_m \end{Bmatrix} = \sum_{n=1}^{\infty}\sum_{q=0}^{\infty} \begin{Bmatrix} \bar{U}_n(r) \\ \bar{\phi}_n(r) \\ \bar{\phi}^*_{m,n}(r) \end{Bmatrix} \cos(n\theta)\sin\left(\tfrac{q\pi z}{\lambda L}\right) (m = o, i), \tag{20}$$

where both n and q are integers, representing the circumferential and axial wave numbers, respectively. We can also treat $k = \frac{q\pi}{\lambda L}$ as the axial wave number, which usually is not an integer. By substituting Eq. (20) into Eq. (18), we obtain

$$\left(\Lambda + \eta_4^2\right)\bar{\psi}_n = 0, \tag{21}$$

$$\left[(c_{11} - c_{13} - c_{551})\Lambda - c_{553}k^2\right]\bar{G}_n - (e_{31} + e_{15})k\bar{\phi}_n + \bar{\dot{p}}_n = 0,$$
$$\left[c_{552}\Lambda - (c_{33} - c_{13} - c_{551})k^2\right]\bar{U}_n + \left(e_{15}\Lambda - e_{33}k^2\right)\phi_n + k\bar{\dot{p}}_n = 0,$$
$$\left[e_{15}\Lambda - (e_{33} - e_{31} - e_{15})k^2\right]\bar{U}_n - \left(\varepsilon_{11}\Lambda - \varepsilon_{33}k^2\right)\bar{\phi}_n = 0,$$
$$-\Lambda\bar{G}_n + k\bar{U}_n = 0, \tag{22}$$

where $\Lambda = \frac{d^2}{dr^2} + \frac{1}{r}\frac{d}{dr} - \frac{n^2}{r^2}$, and $\eta_4^2 = -\frac{c_{553}k^2}{c_{661}}$. Eq. (21) is a Bessel equation of order n, and the solution is

$$\bar{\psi}_n = A_4 J_n(\eta_4 r) + B_4 Y_n(\eta_4 r), \tag{23}$$

where $J_n(\cdot)$ and $Y_n(\cdot)$ are respectively the nth order Bessel functions of the first and second kinds. Similarly, for Eq. (22), the solution can be sought by assuming

$$\begin{Bmatrix} \bar{G}_n \\ \bar{U}_n \\ \bar{\phi}_n \\ \bar{\dot{p}}_n \end{Bmatrix} = J_n(\eta r)\begin{Bmatrix} C_1 \\ C_2 \\ C_3 \\ C_4 \end{Bmatrix} + Y_n(\eta r)\begin{Bmatrix} D_1 \\ D_2 \\ D_3 \\ D_4 \end{Bmatrix}, \tag{24}$$

where C_j and $D_j (j = 1 \sim 4)$ are constants to be determined, and η, according to the non-trivial solution of the system, is determined by the following characteristic equation

$$\eta^6\left(e_{15}^2 + c_{552}\varepsilon_{11}\right) - \eta^4 k^2[2e_{15}(e_{15} + e_{31} - e_{33}) - \varepsilon_{11}(c_{11} - 2c_{13} + c_{33} - 2c_{551}) - c_{552}\varepsilon_{33}]$$
$$+\eta^2 k^4\left[(e_{15} + e_{31} - e_{33})^2 + c_{553}\varepsilon_{11} + \varepsilon_{33}(c_{11} - 2c_{13} + c_{33} - 2c_{551})\right] + c_{553}\varepsilon_{33}k^6 = 0. \tag{25}$$

Generally, Eq. (25) has three pairs of roots in the way of $\pm\eta_j$ $(j = 1, 2, 3)$, for which the Bessel functions $Z_n(\eta_j r)$ and $Z_n(-\eta_j r)$ $(Z = J \text{ or } Y)$ with linear dependence on each other are both the roots of Eq. (22). For simplicity, we may choose three of them in such a way that $\mathrm{Re}[\eta_j] > 0$, or $\mathrm{Re}[\eta_j] = 0$ and $\mathrm{Im}[\eta_j] > 0$ to construct the complete solution, which is written as

$$\begin{Bmatrix} \bar{G}_n \\ \bar{U}_n \\ \bar{\phi}_n \\ \bar{\dot{p}}_n \end{Bmatrix} = \sum_{j=1}^{3}\begin{Bmatrix} 1 \\ \zeta_{1j} \\ \zeta_{2j} \\ \zeta_{3j} \end{Bmatrix}\left[A_j J_n(\eta_j r) + B_j Y_n(\eta_j r)\right] \tag{26}$$

where ζ_{ij} are ratios between the constants and can be obtained as

$$\zeta_{1j} = -\frac{\eta_j^2}{k}, \zeta_{2j} = \frac{e_{15}\eta_j^2 + (e_{33} - e_{31} - e_{15})k^2}{\varepsilon_{11}\eta_j^2 + \varepsilon_{33}k^2}\zeta_{1j},$$
$$\zeta_{3j} = -\frac{1}{k}\left\{\left[-c_{552}\eta_j^2 - (c_{33} - c_{13} - c_{551})k^2\right]\zeta_{1j} - \left(e_{15}\eta_j^2 + e_{33}k^2\right)\zeta_{2j}\right\}. \tag{27}$$

Please cite this article as: Y. Su et al., On buckling of a soft incompressible electroactive hollow cylinder, International Journal of Solids and Structures (2016), http://dx.doi.org/10.1016/j.ijsolstr.2016.07.008

With the solutions in Eqs. (23) and (26), the incremental stresses, electric displacements and electric fields in the hollow cylinder and vacuum space are readily obtainable by using Eqs. (17) and (10) in turn.

As mentioned before, the boundary conditions involve the electric potential ϕ_m^* in the exterior space that is governed by Eq. (16). Using the solution in Eq. (20) leads to a modified Bessel equation as

$$\left(\Lambda - k^2\right)\bar{\phi}_m^* = 0 \quad (m = o, i), \tag{28}$$

to which the solution is

$$\bar{\phi}_o^* = A_o^* K_n(kr), \quad \bar{\phi}_i^* = A_i^* I_n(kr), \tag{29}$$

where A_o^* and A_i^* are unknown constants, while $I_n(\cdot)$ and $K_n(\cdot)$ are respectively the nth order modified Bessel functions of the first and second kinds.

Inserting the solution of ϕ_m^* into the boundary conditions in Eqs. (12) and (13) yields a system of ten linear homogeneous equations with respect to $A_j, B_j (j = 1-4)$ and $A_m^* (m = o, i)$. Non-trivial solutions for the cylinder's buckling behavior require the determinant of the coefficient matrix for the linear system to vanish, i.e.,

$$|\mathbf{d}| = 0. \tag{30}$$

The elements d_{ij} of the matrix $\mathbf{d}$ are given in Appendix C. Eq. (30) is the so-called bifurcation equation that identifies the critical pre-stretch λ_c which announces the arising of buckling phenomenon.

4. Illustrative example

Application of the above formulations relies on the choice of the energy density function $W(\mathbf{F}, \mathbf{D}_l)$ for the material. As an illustrative example, the energy density function is assumed in the following amendatory neo-Hookean model (Dorfmann and Ogden, 2010)

$$W = \frac{1}{2}\mu(I_1 - 3) + \frac{1}{\varepsilon_0}(\alpha I_4 + \beta I_5), \tag{31}$$

where μ is the initial shear modulus and α, β are two dimensionless electroelastic coupling parameters. The first term is the energy density function of an incompressible neo-Hookean solid, while the second term accounts for the interaction between the elastic deformation and the electric field. For the current hollow cylinder, the invariants in Eq. (31) are determined by

$$I_1 = \lambda^2 + \frac{2}{\lambda}, \quad I_4 = \lambda^{-2} D_z^2, \quad I_5 = \lambda^{-4} D_z^2. \tag{32}$$

The corresponding effective material parameters are obtained by substituting Eqs. (2) and (31) into Eq. (A7) as

$$\begin{aligned}
c_{11} &= c_{661} = \mu\lambda^{-1}, c_{12} = c_{13} = c_{662} = 0, c_{33} = \mu\lambda^2 + 2\varepsilon_0^{-1}\beta D_z^2 \\
&\quad - \frac{8\varepsilon_0^{-1}\beta^2 D_z^2}{\alpha\lambda^{-2} + \beta}, \\
c_{551} &= -\frac{2\varepsilon_0^{-1}\beta^2 D_z^2}{\alpha\lambda + \beta}, c_{552} = \mu\lambda^{-1} + c_{551}, c_{553} = \mu\lambda^2 + 2\varepsilon_0^{-1}\beta D_z^2 \\
&\quad + c_{551}, \\
\varepsilon_{11} &= \frac{\varepsilon_0}{2(\alpha\lambda + \beta)}, \varepsilon_{33} = \frac{\varepsilon_0}{2\left(\alpha\lambda^{-2} + \beta\right)}, \\
e_{15} &= -\frac{\beta D_z}{\alpha\lambda + \beta}, e_{31} = 0, e_{33} = -\frac{2\beta D_z}{\alpha\lambda^{-2} + \beta}.
\end{aligned} \tag{33}$$

Generally, the electroelastic coupling parameters α and β are positive (Ogden, 2009). We can see directly from Eq. (33) that the permittivity ε_{33} decreases as the compression increases (*i.e.*, λ decreases), which is consistent with the experimental observations for a dielectric plate (Wissler and Mazza, 2007). The permittivity will be always constant during the deformation for $\alpha = 0$ and the dielectric behavior of the elastomer is liquidlike. Such an energy function corresponds to the so-called ideal dielectric elastomer (Zhao and Suo, 2007).

For the sake of presentation, the following dimensionless variables are introduced,

$$\kappa = kr_o, \delta = \frac{D_z}{\sqrt{\mu\varepsilon_0}}, \bar{\eta}_j = \eta_j r_o (j = 1, 2, 3, 4). \tag{34}$$

The roots of Eq. (25) are then given by

$$\bar{\eta}_1 = i\kappa, \bar{\eta}_2 = i\kappa\lambda^{3/2}, \bar{\eta}_3 = i\kappa\sqrt{\frac{\alpha + \beta\lambda^{-1} + 2\alpha\beta\delta^2\lambda^{-2}}{\beta\lambda^{-1} + \alpha\lambda^{-3}}}, \tag{35}$$

and $\bar{\eta}_4$ can be calculated as

$$\bar{\eta}_4 = i\kappa\sqrt{\lambda^3 + \frac{2\alpha\beta\lambda^2\delta^2}{\alpha\lambda + \beta}}. \tag{36}$$

Accordingly, Eq. (4) further simplifies to

$$D_z = \frac{\varepsilon_0}{2\left(\alpha\lambda^{-2} + \beta\right)} E_z = \varepsilon E_z. \tag{37}$$

5. Results and discussions

The impact of exterior electric field in vacuum on the responses of traditional piezoelectric materials is relatively small (Chen, 1973). However, for soft electroactive materials, the exterior electric field may play a key role, as shown in our previous study on wave propagation in cylinders (Su et al., 2016). In this section, we will analyze the buckling behavior of a soft electroactive cylinder with or without the effect of exterior electric field in a comparison manner through numerical calculations.

5.1. Including exterior electric field

Here, we consider an electroactive cylinder immersed in a uniform exterior electric field normal to its end faces. Then, the *hydrostatic pressure* is $p = \mu\lambda^{-1} + 2\mu(\alpha\lambda^{-2} + \beta)^2\delta^2$, and the non-dimensional axial load $s = g/\mu$ (here g is the applied compressive load) may be obtained from the boundary condition $\tau_{zz} = \tau_{ozz}^* - g(z = 0, l)$ as

$$s = -\lambda^2 + \lambda^{-1} + 4\delta^2(\alpha\lambda^{-2} + \beta)^2 - 2\beta\delta^2. \tag{38}$$

This equation reveals the effects of the applied compressive load and uniform longitudinal electric displacement on the deformation of the cylinder. Under the stimulus of the initial longitudinal biasing electric displacement only, i.e., $g = 0$, the axial stretch λ of the cylinder may be determined through the equation

$$-\lambda^2 + \lambda^{-1} + 4\delta^2(\alpha\lambda^{-2} + \beta)^2 - 2\beta\delta^2 = 0, \tag{39}$$

which is a sextic equation of λ and is difficult to obtain analytical solutions. Eq. (39) also indicates that the relation between the stretch λ and stimulus δ depends on both α and β. In practice, however, it has been widely approved that the model of ideal dielectric elastomers, i.e., $\alpha = 0$ in Eq. (31), is accurate enough to predict the response of a wide range of soft electroactive materials (Zhao and Suo, 2007; Shmuel et al., 2012). Therefore, we only focus on the buckling behavior of hollow cylinders of ideal dielectric elastomer ($\alpha = 0$), for which Eq. (39) is reduced to

$$\lambda^2 - \lambda^{-1} = 2\beta\delta^2(2\beta - 1). \tag{40}$$

For this case, it is deterministic that $\lambda > 1$ for $\beta > 0.5$, $\lambda < 1$ for $\beta < 0.5$, and we always have $\lambda = 1$ for $\beta = 0.5$.

Please cite this article as: Y. Su et al., On buckling of a soft incompressible electroactive hollow cylinder, International Journal of Solids and Structures (2016), http://dx.doi.org/10.1016/j.ijsolstr.2016.07.008

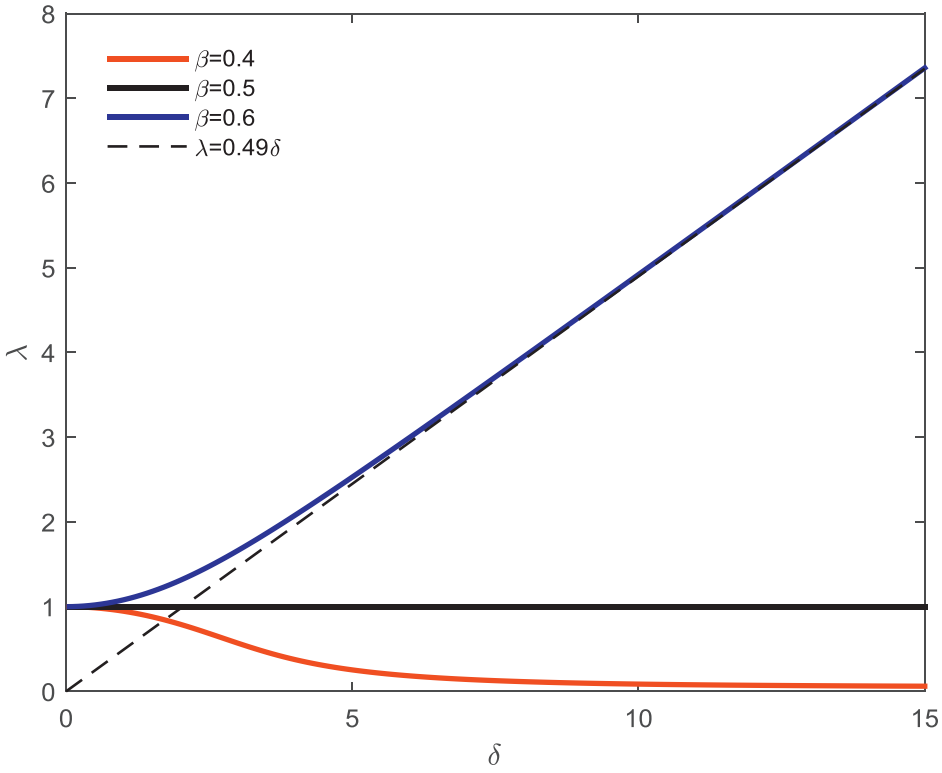

Fig. 1. Plots of λ versus δ for a hollow cylinder of ideal dielectric elastomer ($\alpha = 0$) for various β. The dashed line represents the asymptote of the curve for $\beta = 0.6$.

Note from Eq. (35) that, for ideal dielectric elastomers ($\alpha = 0$), repeated roots of the characteristic Eq. (25) are present, i.e., $\tilde{\eta}_1 = \tilde{\eta}_3$. Thus, a solution in a form different from Eq. (24) is required (Dorfmann and Ogden, 2014), which will change the related formulations. Physically, however, the behavior of the cylinder should be continuous when the parameter α reduces from a very small number down to zero. This implies that we may take a sufficiently small α (e.g. $\sim 10^{-6}$) instead of $\alpha = 0$ to avoid the repeated roots. This has been validated through comprehensive numerical calculations. Then, the solution (24) can be still used for ideal dielectric elastomers but based on a very close hypothetical non-ideal model.

Fig. 1 displays the stretch λ as a function of the normalized biasing electric displacement δ according to Eq. (40) for ideal dielectric elastomers. It is shown that the hollow cylinder is compressed for $\beta < 0.5$ and stretched for $\beta > 0.5$ in the presence of an electric displacement. When $\beta = 0.5$, the cylinder remains undeformed ($\lambda = 1$) after the voltage is applied, that is the electric displacement δ induces no deformation. Thus, whether the applied electric displacement compresses, stretches, or poses no deformation to the ideal electroactive material depends on the material constants, which is different from the predictions (Zhao and Suo, 2008) ignoring the influences of the exterior electric field. Interesting phenomena are observed that, when the applied electric displacement δ approaches infinity, the cylinder is almost compressed to an ultrathin film for $\beta < 0.5$, but, on the contrary, is stretched almost in a linear manner versus δ for $\beta > 0.5$. The latter may also be deduced from the solution to Eq. (40) which is approximately $\lambda = \delta\sqrt{2\beta(2\beta-1)}$ for $\beta > 0.5$ and large δ. In other words, the relative stretch λ/δ remains constant as $\sqrt{2\beta(2\beta-1)}$ irrespective of the applied electric displacement, as shown in Fig. 1 by the dashed line for $\beta = 0.6$. This property may be utilized to check if $\beta > 0.5$ and determine the value of β experimentally.

Similarly, for electroactive material with $\beta < 0.5$ under sufficiently large electric field, it will be compressed dramatically that the portion of λ^2 can be discarded compared to λ^{-1}. Then Eq. (40) approximately reduces to $\lambda^{-1/2} = \delta\sqrt{2\beta(2\beta-1)}$, as depicted in Fig. 2 by the dashed line, shows a linear relationship between $\lambda^{-1/2}$ and δ for large δ. This provides an effective means to measure the value of β for $\beta < 0.5$.

The buckling behavior of the cylinder of ideal dielectric elastomer is governed by the characteristic Eq. (30), from which the critical stretch λ_c may be determined as

$$\lambda_c = \lambda_c(\kappa,\ n;\ \beta,\ \delta,\ \nu). \tag{41}$$

This gives the scaling law between the critical buckling stretch λ_c and the wave number κ, which implies that the relation $\lambda_c \sim \kappa$ for a certain buckling mode n may be uniquely determined once the radius ratio ν, the electroelastic coupling parameter β, and the non-dimensional biasing electric displacement δ are fixed. That is, the scaling of $\lambda_c \sim \kappa$ with fixed values of β, n, and δ will not be influenced by the initial shear modulus μ and the permittivity constants ε_0, but only relies on the relative thickness of the cylinder ν.

Now, the buckling behavior of the cylinder due to the biasing electric field will be investigated through numerical calculations. Examples are performed according to whether the cylinder is initially compressed with $\beta = 0.4$ or stretched with $\beta = 0.6$. For ease of reference, we designate λ_0 as the prestretch due to the biasing electric displacement δ in the absence of mechanical loads. Variations of the normalized critical stretch λ_c/λ_0 versus the normalized wave number κ will be analyzed. All results will be given for the lowest five orders of circumferential buckling modes.

Firstly, the critical stretch λ_c/λ_0 versus κ is analyzed for a cylinder with ν=0.5 and subjected to no biasing electric displacement, i.e., $\delta = 0$. For this case, the stretch due to $\delta = 0$ is $\lambda_0 = 1$ as shown in Fig. 1. Fig. 3 exhibits the $\lambda_c/\lambda_0 \sim \kappa$ curves that are similar to the classical features of the buckling of a purely elastic cylindrical shell (Pan and Beatty, 1997; Goriely et al., 2008). It can be seen that the Euler buckling ($n = 1$) occurs first during compression for slender cylinder with $\kappa < 5.5$ while the first barrelling mode ($n = 0$)

Please cite this article as: Y. Su et al., On buckling of a soft incompressible electroactive hollow cylinder, International Journal of Solids and Structures (2016), http://dx.doi.org/10.1016/j.ijsolstr.2016.07.008

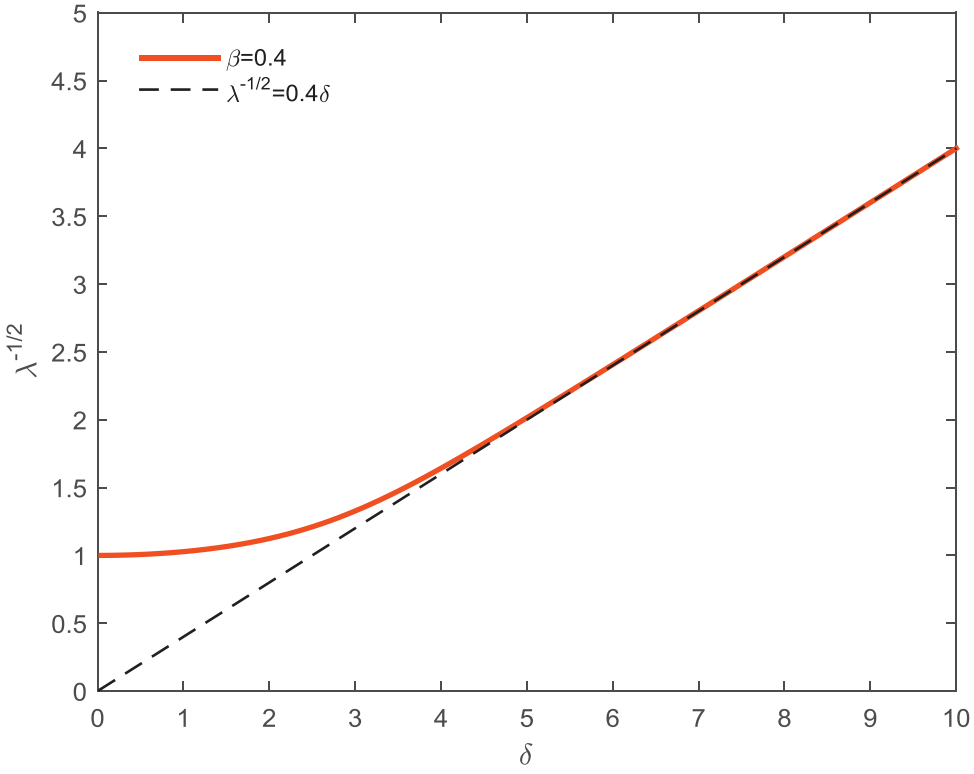

Fig. 2. Plots of $\lambda^{-1/2}$ versus δ for a hollow cylinder of ideal dielectric elastomer ($\alpha = 0$) for $\beta = 0.4 < 0.5$. The dashed line is the asymptote of the solid curve.

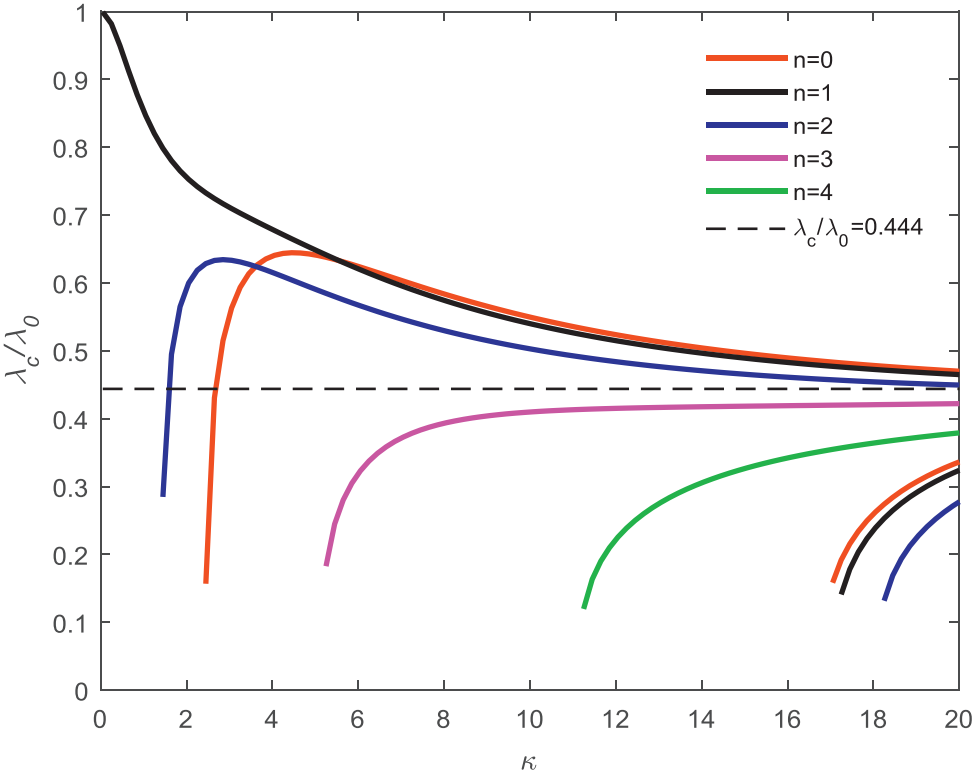

Fig. 3. Plots of the critical stretch λ_c/λ_0 ($\lambda_0 = 1$) versus κ for a hollow cylinder with $\nu = 0.5$ without the stimulus of initial biasing electric displacement ($\delta = 0$). The dashed line is the asymptote corresponding to a half-space.

Please cite this article as: Y. Su et al., On buckling of a soft incompressible electroactive hollow cylinder, International Journal of Solids and Structures (2016), http://dx.doi.org/10.1016/j.ijsolstr.2016.07.008

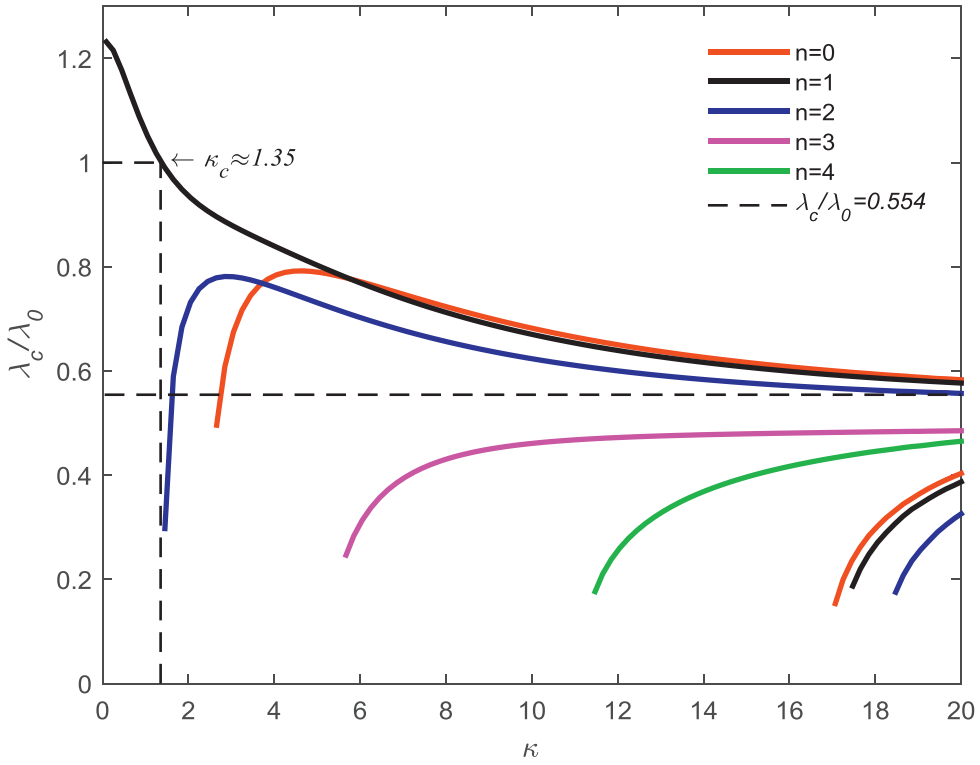

Fig. 4. Plots of λ_c/λ_0 versus κ for a range of mode numbers $n = 0, 1, 2, 3, 4$ for a hollow cylinder with $\alpha = 0, \beta = 0.4$ and $\nu = 0.5$ subjected to $\delta = 2$. The horizontal dashed line is the asymptote corresponding to a half-space.

becomes dominant for short cylinder with $\kappa > 5.5$. Special attention should be paid to the buckling behavior of short cylinders with $\kappa > 5.5$ for which the mode curves of $n = 0$ and $n = 1$ are so close that a slight additional axial compression is likely to drive the cylinder from the first barrelling mode into the Euler buckling or some combination of both modes. Both mode curves decrease together monotonically to the asymptotic value $\lambda_c = 0.444$, which corresponds to surface instability of a compressed half-space (Wilkes, 1955). This asymptotic value is different from the critical compression stretch $\lambda_c = 0.5437$ for buckling instability of a neo-Hookean elastic half-space obtained by Dorfmann and Ogden (2010) and Biot (1963) who considered a plane-strain state with a deformation gradient tensor of $\mathbf{F} = \mathrm{diag}[\lambda\, \lambda^{-1}\, 1]$. The critical stretches λ_c for other modes ($n \geq 2$) are always beneath those for the first barrelling mode ($n = 0$) and the Euler buckling mode ($n = 1$), implying the requirement of a larger compression load to induce them. One should notice that for short cylinder with large κ, multiple solution curves appear (Pan and Beatty, 1997). These curves should be ignored since the major instability curves at which instability first occurs are the upper branch curves.

Figs. 4 and 5 present the effect of the applied electric displacement $\delta = 2$ on the stability of an electroactive cylinder respectively with ν=0.5 and ν=0.8 for $\beta = 0.4$. For $\lambda_c/\lambda_0 > 1$, the cylinder buckles immediately once an electric displacement $\delta = 2$ is applied and a tensile mechanical load is necessary to prevent the buckling. However, only Euler buckling mode ($n = 1$) is induced for slender cylinders with $\kappa < 1.35$ when ν=0.5 (Fig. 4). In contrast, for cylinders with ν=0.8, a wider range of wave number (e.g. $0 < \kappa < 8.27$) will result in immediate buckling due to the electrical load ($\lambda_c/\lambda_0 > 1$), but the critical buckling mode varies among $n = 1$, $n = 2$ and $n = 0$ versus κ (Fig. 5). As the wave number κ increases such that $\lambda_c/\lambda_0 < 1$, the applied electric field is not adequate any more to induce buckling but an additional axial compression is required to destabilize the cylinder, that is, the cylinder can bear an additional axial compression until the buckling occurs. In Figs. 4 and 5, κ_c represents the transition from unstable to stable configuration for the initially undeformed cylinder with $\lambda = 1$ under the application of the electric field. It may be deduced that further increasing of δ will result in larger values of κ_c and a larger axial tension is needed to prevent instability of the slender cylinder with $\kappa < \kappa_c$.

The $\lambda_c/\lambda_0 \sim \kappa$ curves in Figs. 4 and 5 for various buckling modes have cross points at certain wave number, which indicates that the hollow cylinder will shift between different buckling modes as the radius ratio ν or wave number varies. In addition, larger radius ratios result in more cross points or more frequent shift of buckling modes. To further investigate this phenomenon, we extract the wave number corresponding to the cross point of two buckling modes in the $\lambda_c/\lambda_0 \sim \kappa$ plots for a continuous spectrum of radius ratio ν, and plot the $\kappa \sim \nu$ relation in Fig. 6 to achieve the phase diagram of buckling modes. The $\kappa - -\nu$ plane is divided into various regions by the buckling mode number n. The Euler buckling ($n = 1$) always occurs first as κ increases irrespective of the radius ratio ν, and, in general, the Euler buckling ($n = 1$) is dominant for slender cylinders (small κ) while the first barrelling mode ($n = 0$) is dominant for short cylinders (large κ). For thick cylinders with $\nu < 0.65$, only the first barrelling mode ($n = 0$) and the Euler buckling mode ($n = 1$) may occur. More buckling modes appear as ν exceeds 0.65, and the buckling modes shift follows the rule of $n = 1 \to 2 \to \cdots \to n \to \cdots \to 1 \to 0$ for a certain value of ν as κ increases, which indicates more complicated buckling behavior for thinner cylinders. When the biasing electric displacement δ shifts from 0 to 2, there is almost no change in the number of divided regions on the $\kappa \sim \nu$ diagram, but there is only a slight increment in the wave number, implying that the applied electric displacement delays the shift of buckling

Please cite this article as: Y. Su et al., On buckling of a soft incompressible electroactive hollow cylinder, International Journal of Solids and Structures (2016), http://dx.doi.org/10.1016/j.ijsolstr.2016.07.008

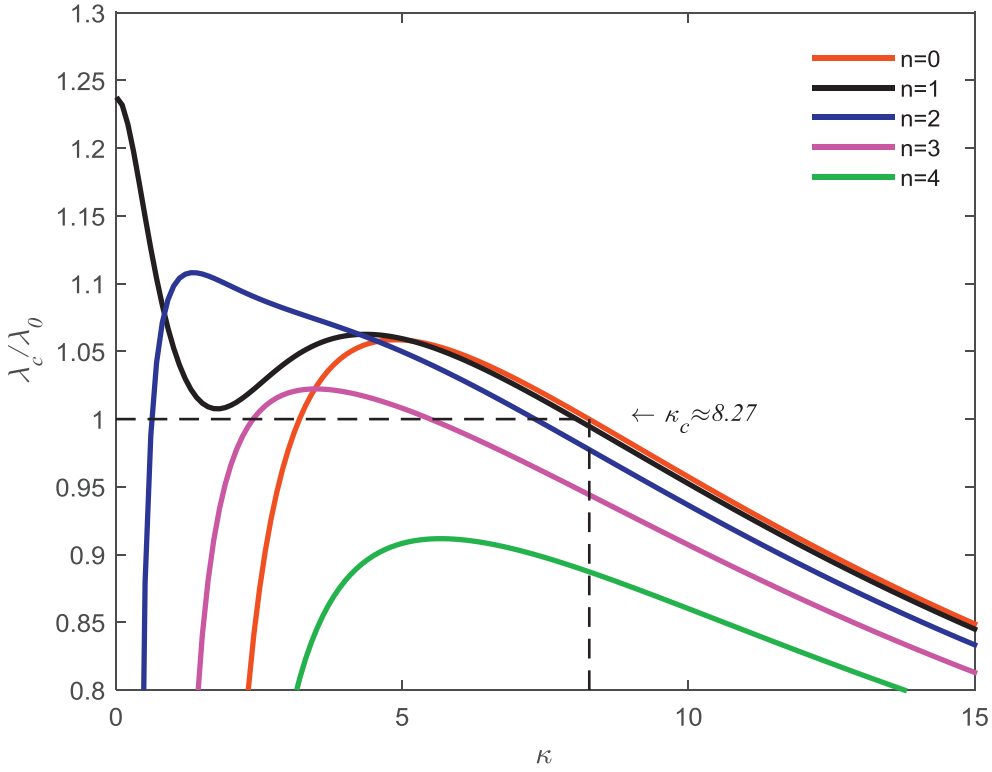

Fig. 5. Plots of λ_c/λ_0 versus κ for a range of mode numbers $n = 0, 1, 2, 3, 4$ for a hollow cylinder with $\alpha = 0$, $\beta = 0.4$ and $\nu = 0.8$ subjected to $\delta = 2$.

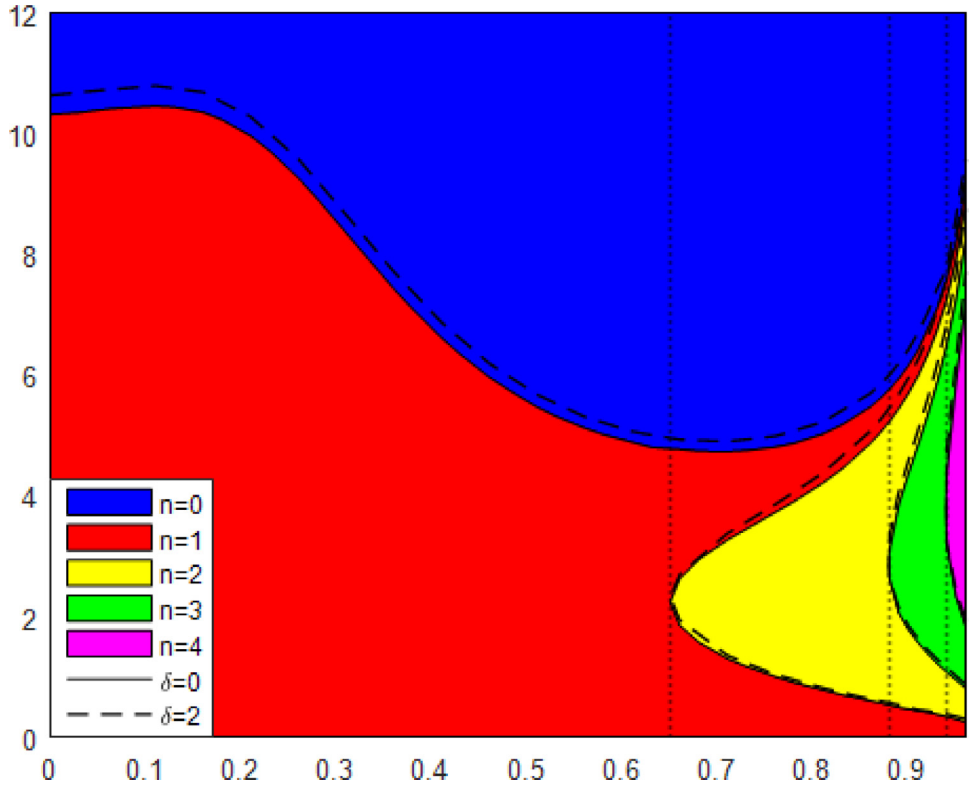

Fig. 6. Phase diagram of buckling modes: solid – $\alpha = 0, \beta = 0.4, \delta = 0$; dashed – $\alpha = 0, \beta = 0.4, \delta = 2$. The vertical dotted lines indicate the smallest radius ratio at which transition from one buckling mode to another occurs when the axial wave number is not very large.

Please cite this article as: Y. Su et al., On buckling of a soft incompressible electroactive hollow cylinder, International Journal of Solids and Structures (2016), http://dx.doi.org/10.1016/j.ijsolstr.2016.07.008

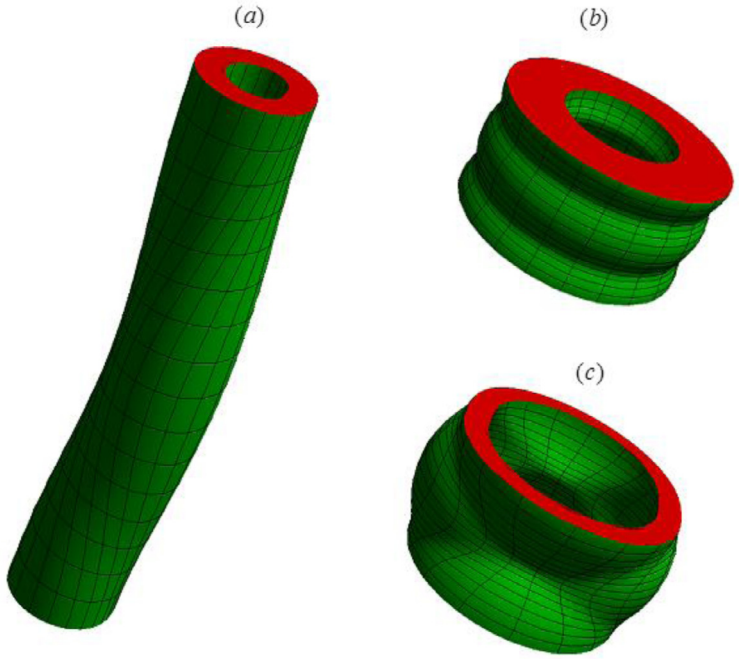

Fig. 7. Buckling mode shapes for a hollow cylinder: (a) $\kappa = 0.3, n = 1, \nu = 0.5, q = 1$, (b) $\kappa = 6, n = 0, \nu = 0.5, q = 2$and (c) $\kappa = 3, n = 2, \nu = 0.8, q = 1$.

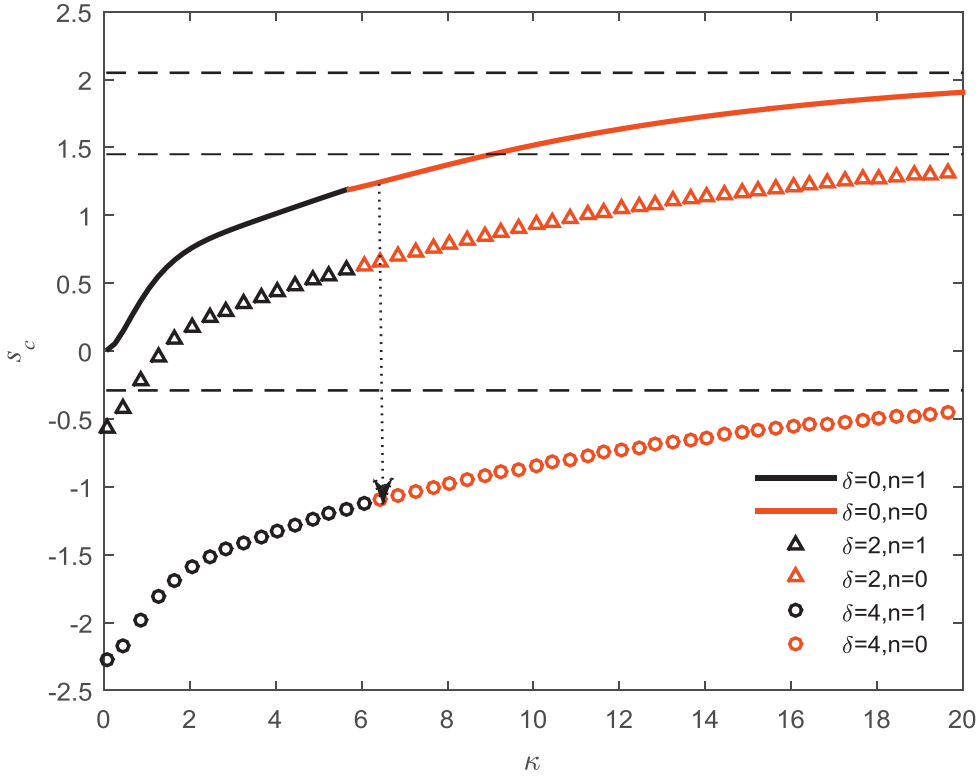

Fig. 8. Plots of s_c versus κ for a hollow cylinder with $\alpha = 0, \beta = 0.4$ and $\nu = 0.5$ subjected to $\delta = 0, 2, 4$, respectively. The dashed lines are the asymptotes of the respective curves.

mode as κ increases. In addition, the role of biasing electric field on delaying the mode shift becomes weaker as ν increases.

Once κ, R_o, R_i and δ are prescribed, the critical stretch λ_c and the buckling modes of the cylinder may be determined as shown in Fig. 7. The length of the cylinder can be determined by $L = \frac{q\pi R_o}{\kappa}\lambda_{cr}^{-3/2}$.

From the results presented above, we can expect that for $\kappa \to \infty$, the first barrelling mode ($n = 0$) occurs first during compression. From Eq. (30) for ideal dielectric elastomers ($\alpha = 0$), letting $\kappa \to \infty$ and $n = 0$, λ approaches a value which is the positive root of the equation

$$(1+2\beta)\left(\lambda^{9/2}+\lambda^3+3\lambda^{3/2}-1\right)-\delta^2(1-2\beta)^2\left(\lambda+\lambda^{5/2}\right)=0, \tag{42}$$

Please cite this article as: Y. Su et al., On buckling of a soft incompressible electroactive hollow cylinder, International Journal of Solids and Structures (2016), http://dx.doi.org/10.1016/j.ijsolstr.2016.07.008

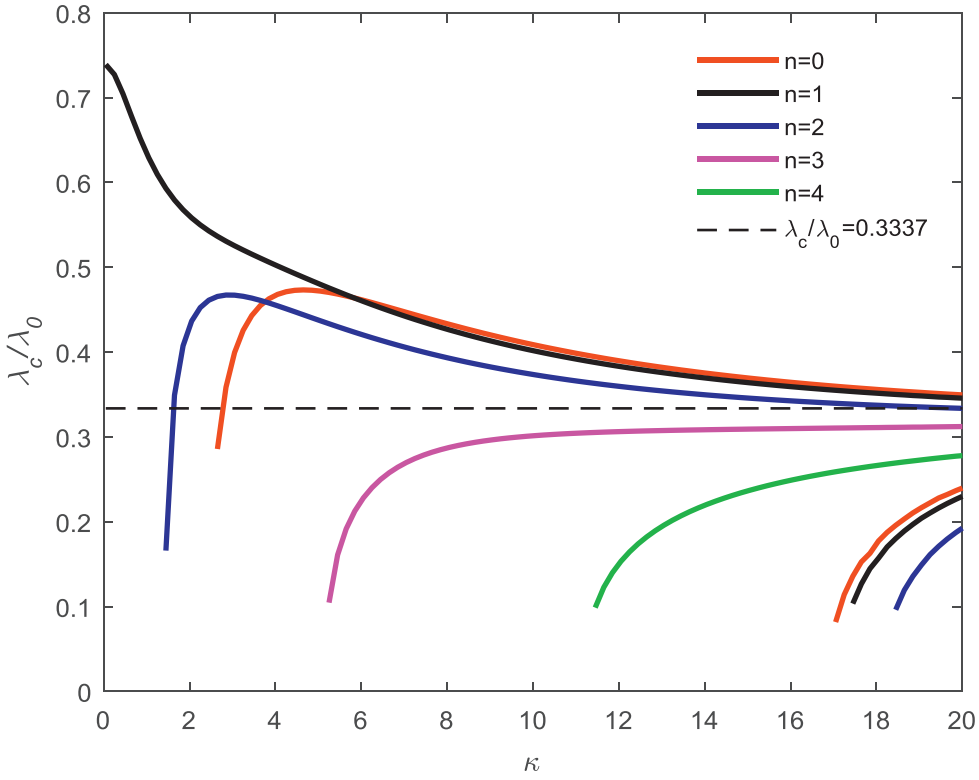

Fig. 9. Plots of λ_c/λ_0 versus κ for a range of mode numbers $n = 0, 1, 2, 3, 4$ for a hollow cylinder with $\alpha = 0$, $\beta = 0.6$ and $\nu = 0.5$ subjected to $\delta = 2$.

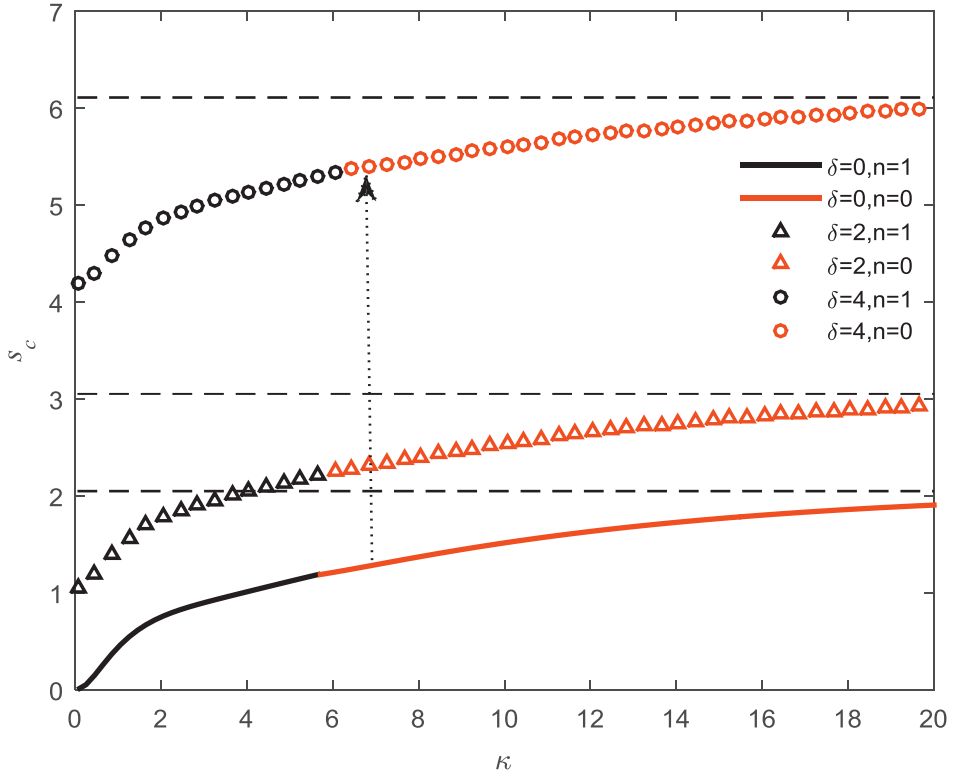

Fig. 10. Plots of s_c versus κ for a hollow cylinder with $\alpha = 0$, $\beta = 0.6$ and $\nu = 0.5$ subjected to $\delta = 0, 2, 4$, respectively.

and is irrespective of ν. It shows again that for ideal electroactive material with $\beta = 0.5$, biasing electric field imposes no effect on the buckling behavior. Furthermore, if omitting the effect of biasing electric fields ($\delta = 0$), we obtain

$$\lambda^{9/2} + \lambda^3 + 3\lambda^{3/2} - 1 = 0, \tag{43}$$

with the positive real root $\lambda = 0.444$, the same as the critical compression for buckling instability of a neo-Hookean elastic half-space (Wilkes, 1955), just as expected.

The applied critical compressive load which induces buckling of the cylinder may be determined according to Eq. (38). Fig. 8 il-

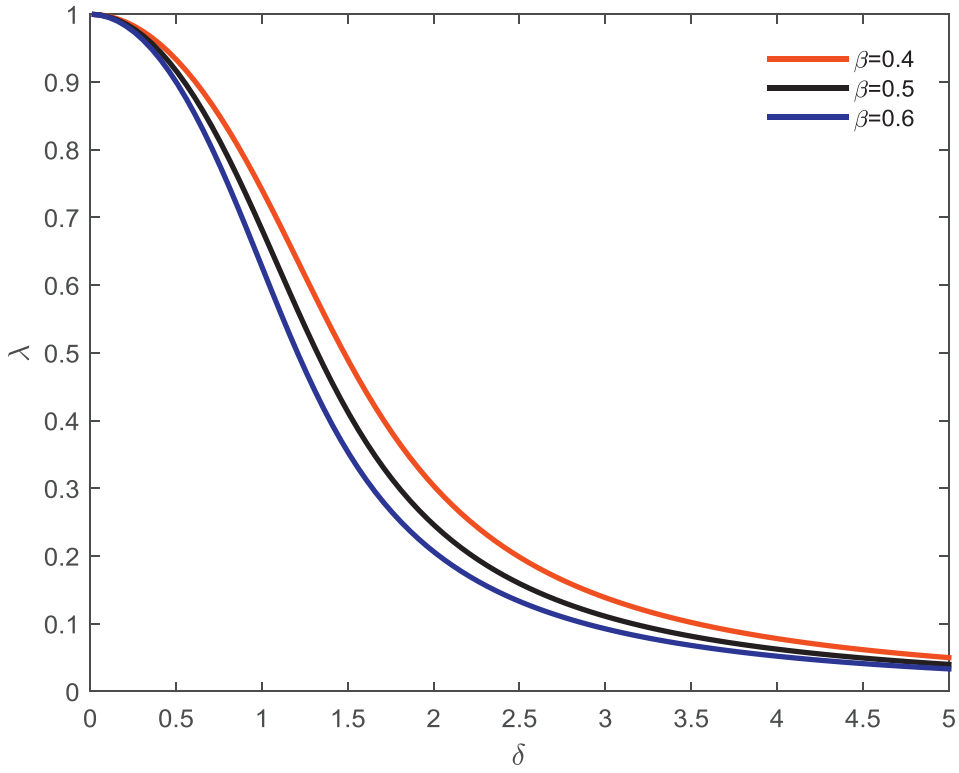

Fig. 11. Plots of λ versus δ for $\alpha = 0$ and $\beta = 0.4, 0.5, 0.6$.

lustrates the dependence of the critical compressive load s_c on the wave number κ for various applied electrical displacement δ based on the energy function (31) with $\alpha = 0$, $\beta = 0.4$ and a radius ratio $\nu = 0.5$. It is seen again that, as κ increases, the Euler buckling ($n = 1$ with black segment or markers) occurs first and then follows the first barrelling mode ($n = 0$ with red segment or markers). The critical compressive load increases monotonically to an asymptotic value which corresponds to the critical load under which the surface of the electroactive half-space will become unstable. For the purely mechanical loading case ($\delta = 0$), the $s_c \sim \kappa$ curve is always above zero which implies that an axial compressive load is needed to buckle the hollow cylinder no matter how slender the cylinder is. Once the electrical load is applied, part of the $s_c \sim \kappa$ curve for thin cylinder with $\kappa < \kappa_c$ is below zero while the remaining section of the curve is above zero. That is, for slender cylinder with small κ, an electric field only will buckle the cylinder and a tensile force is needed to prevent the buckling, while, for thick cylinder with large κ, the applied electric field will not buckle the cylinder and a compressive load is allowed until the buckling occurs, coinciding with the results presented in Figs. 4 and 5. As the applied electric displacement δ becomes large enough, the critical loading s_c is always below zero for all values of κ, see the curve of $\delta = 4$ for example. This means that the applied electric displacement buckles the cylinder irrespective of its length and a tensile loading is always needed to keep its stability. These results indicate that the ideal dielectric cylinder (with $\alpha = 0, \beta = 0.4$ here) becomes more apt to buckle when the applied electric field gets stronger.

Fig. 9 exhibits the $\lambda_c/\lambda_0 \sim \kappa$ curves of an ideal electroactive cylinder with $\nu = 0.5$ due to an applied electric displacement $\delta = 2$ for $\beta = 0.6$, while Fig. 10 displays the corresponding critical axial load s_c as a function of κ for various δ. Reminder that, for ideal electroactive material with $\alpha = 0, \beta = 0.6$, the applied electric displacement always stretches the cylinder with $\lambda_0 > 1$, that is, the applied electric displacement stabilizes the hollow cylinder. As a result, the critical stretch λ_c/λ_0 causing buckling is always smaller than 1 (see Fig. 9), which indicates that the applied critical compressive load should be large enough to encounter first the prestrech by electric displacement $\delta = 2$ and thereafter to make buckling occur. Accordingly, the critical compressive load s_c is always above zero, and, for a given κ, larger s_c is needed to buckle the hollow cylinder in the presence of a larger electric field. Therefore, the applied electric field considered here plays a positive role and the stability is well enhanced if the cylinder is made of ideal electroactive material with $\beta > 0.5$.

Figs. 2–10 suggest that, for soft electroactive hollow cylinder including the effects of exterior electric field, whether an increasing electric field poses stabilizing or destabilizing influence on the cylinder depends on the selection of the electroelastic coupling parameters. This finding is consistent with the existing theoretical predictions (Dorfmann and Ogden, 2010, 2014).

5.2. Excluding exterior electric field

To make a comparison study on the effects of exterior electric field, we examine here the buckling behavior of electroactive hollow cylinders without considering the electric field in vacuum outside the cylinder. In this circumstance, the boundary conditions reduce to $\tau_{rr} = 0 (r = r_o, r_i)$ in the axisymmetric pre-deformed state, from which the effective hydrostatic pressure is found to be $p = \mu\lambda^{-1}$. Therefore, the boundary conditions at the end faces $\tau_{zz} = -g(z = 0, l)$ give rise to

$$s = g/\mu = -\lambda^2 + \lambda^{-1} - 2\beta\delta^2. \tag{44}$$

This equation suggests that the stretch due to the applied mechanical and electrical loads is independent of α no matter whether the cylinder is made of ideal electroactive material or not. The stretch of the cylinder due to the applied electric displacement can be obtained from Eq. (44) by setting $s = 0$, i.e.,

$$\lambda^2 - \lambda^{-1} + 2\beta\delta^2 = 0. \tag{45}$$

Please cite this article as: Y. Su et al., On buckling of a soft incompressible electroactive hollow cylinder, International Journal of Solids and Structures (2016), http://dx.doi.org/10.1016/j.ijsolstr.2016.07.008

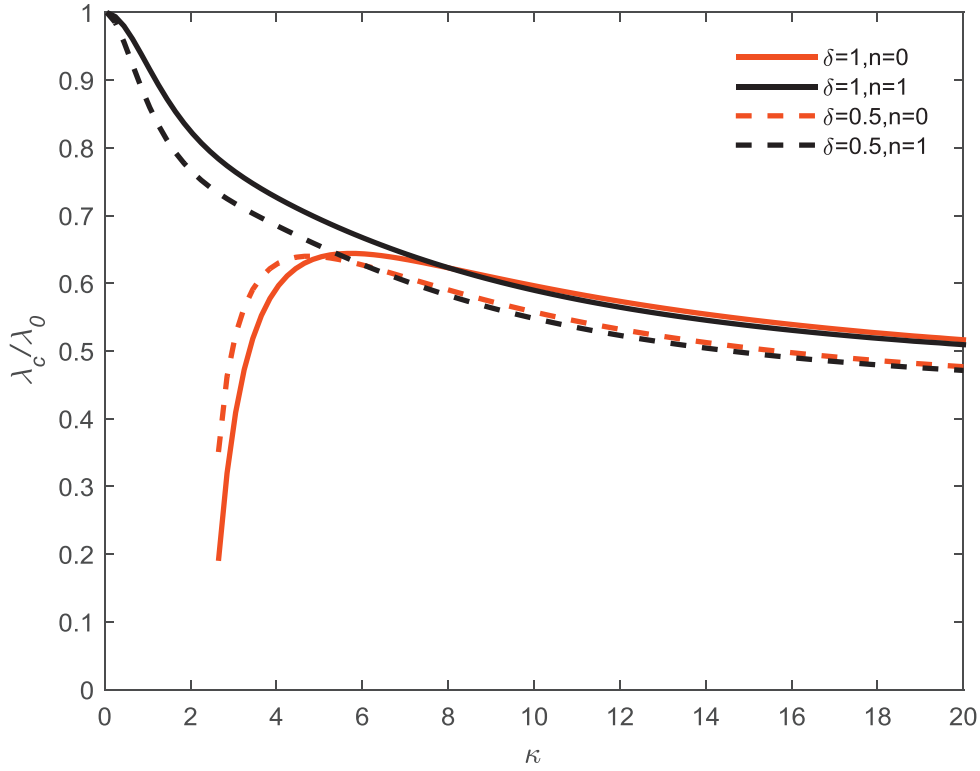

Fig. 12. Plots of λ_c/λ_0 versus κ for mode numbers $n = 0, 1$ for a hollow cylinder with $\alpha = 0, \beta = 0.4$ and $\nu = 0.5$ subjected to $\delta = 0.5, 1$, respectively.

Fig. 11 plots the stretch λ as a function of the normalized biasing electric displacement δ according to Eq. (45) for hollow cylinders made of dielectric elastomer (not necessarily ideal as just noted above) with various parameter β. Similar to the analyses in Su et al. (2016), the applied electric displacement always compresses the hollow cylinder in the absence of exterior electric field, which is quite different from the case including the effects of exterior electric field (see Fig. 1). In addition, the same applied voltage compresses the cylinder more dramatically for a larger β.

Since the exterior electric field is not considered, the potential $\phi_m^*(m = o, i)$ in the vacuum is not included in the boundary conditions for the perturbed motion. Therefore, the solution to $\phi_m^*(m = o, i)$ in Eq. (29) is discarded, and the characteristic equation (30) governing the buckling behavior of the cylinder is reduced to the one involving eight unknowns. In order to directly compare the results to those presented in Section 5.1, we consider again hereafter the buckling of the cylinders made of ideal electroactive materials with $\beta = 0.4$ and $\alpha = 0$ for the case excluding the effects of exterior electric field.

Fig. 12 shows the variations of the normalized critical stretch λ_c/λ_0 against κ for selected values of $\delta = 0.5$ and $\delta = 1$. Only the Euler buckling mode ($n = 1$) and the first barrelling mode ($n = 0$) are discussed here, because, for thick hollow cylinders with $\nu = 0.5$, the curves for other higher order modes are always below these two modes. It is seen that the buckling behavior of the current hollow cylinder is quite different from that including the effects of exterior electric field. For the case of ignoring the exterior electric field, the critical stretch λ_c/λ_0 for the first barrelling mode ($n = 0$) decreases with the applied voltage δ for small values of κ but increases for large values of κ, while that for the Euler buckling mode ($n = 1$) always increases with the applied voltage δ (Fig. 12). This indicates that the cylinder with large κ will be more vulnerable to instability when subject to a higher-level applied voltage. In addition, for the Euler buckling mode ($n = 1$), the critical stretch λ_c/λ_0 always decreases starting from 1 as κ increases when the applied electric field is present. This indicates that mere application of any electric field will not destabilize the hollow cylinder of any thickness if no mechanical load is applied. It is not difficult to understand this because the exterior electric field is ignored so that no total stress occurs in the cylinder as is deduced from the boundary conditions. This conclusion can also be made from Fig. 13 which depicts the associated critical compressive load s_c versus κ for various applied electrical displacement. The critical compressive load s_c is always positive, suggesting that an additional axial compressive load is required to induce buckling. Larger applied electrical displacement requires smaller additional compressive load to buckle the cylinder. In general, from the above comparison between Sections 5.1 and 5.2, the exterior electric field always plays a destabilizing effect, and, this is independent of the value of β.

Similarly, for the case of excluding the exterior electric field, for ideal dielectric elastomers ($\alpha = 0$) as $\kappa \to \infty$, the relation between critical stretch λ_c and electric displacement δ is given by the following equation

$$\lambda^{9/2} + \lambda^3 + 3\lambda^{3/2} - 1 + \beta\delta^2\left(2\lambda^4 + 6\lambda^{5/2} - 4\beta\delta^2\lambda^2 - 4\lambda\right) = 0, \tag{46}$$

which also corresponds to the bifurcation equation of the half - space.

6. Conclusions

In conclusion, we have applied the general nonlinear theory of electroelasticity and the associated linear incremental theory proposed by Dorfmann and Ogden (Dorfmann and Ogden, 2006; Ogden, 2009) to study the buckling behavior of soft incompressible electroactive hollow cylinders subjected to end thrust. Analytical solutions suggest that whether the applied electric field compresses or elongates the cylinder depends on the inclusion/exclusion of exterior electric field and the electromechanical

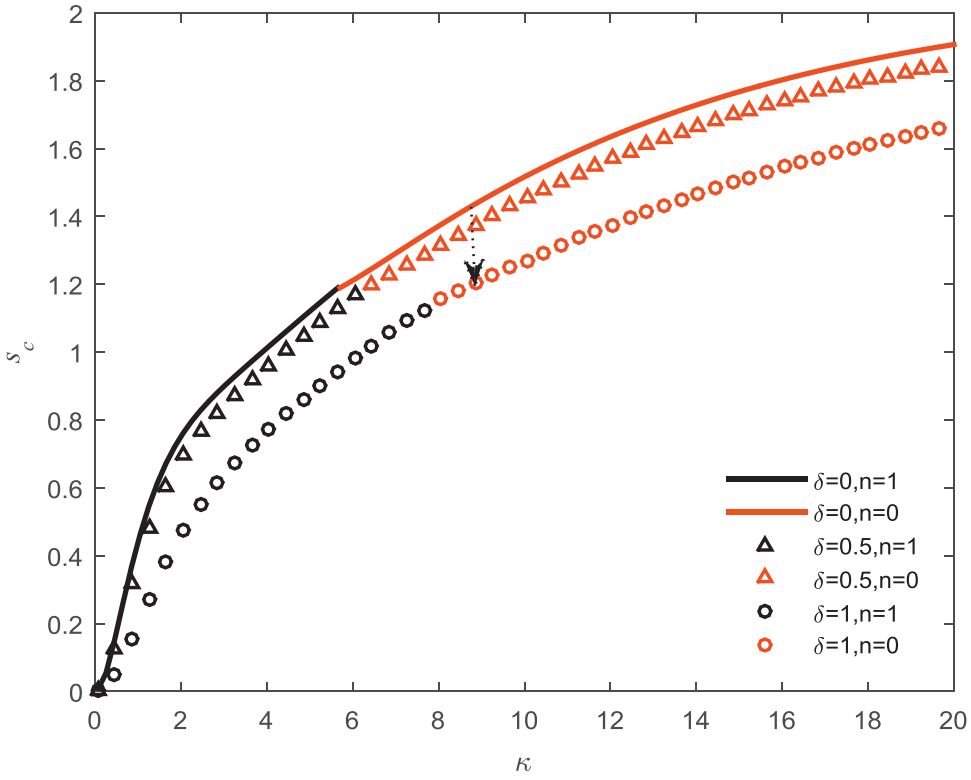

Fig. 13. Plots of s_c versus κ for a hollow cylinder with $\alpha = 0, \beta = 0.4$ and $\nu = 0.5$ subjected to $\delta = 0, 0.5, 1$, respectively.

coupling parameters of the material. In the absence of any biasing field, the general bifurcation relation is identical to that for purely elastic cylinders. Numerical results have shown that the stability is influenced significantly by the biasing fields, material constants, geometrical configuration of the hollow cylinder as well as the exterior electric field. In addition, the instability phenomena of dielectric elastomer also depend highly on material models (Díaz-Calleja et al., 2010), which is not discussed in the present work. A phase diagram has been further constructed to clearly distinguish the dominant buckling modes and to show the transition between them in the $\kappa - -\nu$ plane. All the results may render references for guiding the design and fabrication of tubular electroactive elastomer actuators.

Acknowledgments

This work was supported by the National Natural Science Foundation of China at the Grant nos. 11321202, 11532001, 11322216, and 11172263. It was also partly supported by the Fundamental Research Funds for the Central Universities through Zhejiang University.

Appendix A. Basic equations of nonlinear electroelasticity

A.1. Finite electroelasticity

Consider a continuous electroelastic body subjected to a static finite deformation. The naturally undeformed configuration is denoted by B_r and its boundary by ∂B_r, with $\mathbf{N}$ being the outward unit normal vector. Let B_t denote the corresponding finitely deformed configuration and ∂B_t the deformed boundary with the outward unit normal vector $\mathbf{n}$. For an incompressible material, the nominal stress $\mathbf{T}$ and Lagrangian electric field $\mathbf{E}_l$ during deformation are given by

$$\mathbf{T} = \mathbf{F}^{-1}\tau = \frac{\partial W}{\partial \mathbf{F}} - p\mathbf{F}^{-1}, \quad \mathbf{E}_l = \mathbf{F}^T\mathbf{E} = \frac{\partial W}{\partial \mathbf{D}_l}, \tag{A1}$$

where $\mathbf{F} = \mathrm{Grad}\,\boldsymbol{\chi}$ is the deformation gradient with $\boldsymbol{\chi}$ denoting a continuous and twice differentiable vector function that maps the motion of a material particle at $\mathbf{X}$ in B_r to $\mathbf{x}$ in B_t, i.e., $\mathbf{x} = \boldsymbol{\chi}(\mathbf{X}, t)$ with t being the time variable, $\boldsymbol{\tau}$ the total Cauchy stress tensor, p a Lagrange multiplier associated with the incompressibility constraint, and $\mathbf{E}_l$ and $\mathbf{D}_l$ respectively the Lagrangian counterparts of the electric field vector $\mathbf{E}$ and the electric displacement vector $\mathbf{D}$. The superscripts '−1' and 'T' throughout this paper stand for inverse and transpose of a tensor. In Eq. (A1), $W \equiv W(\mathbf{F}, \mathbf{D}_l)$ is the energy density function defined in the reference configuration, which, in general, is a function of the following six invariants

$$\begin{aligned} &I_1 = \mathrm{tr}\mathbf{c}, I_2 = \frac{1}{2}\left[(\mathrm{tr}\mathbf{c})^2 - \mathrm{tr}(\mathbf{c}^2)\right], I_3 = \det\mathbf{c}, \\ &I_4 = \mathbf{D}_l \cdot \mathbf{D}_l, I_5 = \mathbf{D}_l \cdot (\mathbf{c}\mathbf{D}_l), I_6 = \mathbf{D}_l \cdot (\mathbf{c}^2\mathbf{D}_l), \end{aligned} \tag{A2}$$

where $\mathbf{c} = \mathbf{F}^{\mathrm{T}}\mathbf{F}$ is the right Cauchy–Green tensor, and $I_3 = 1$ for incompressible materials.

In the absence of body forces, free charges and currents, the equations of equilibrium may be written as

$$\mathrm{div}\tau = \mathbf{0}, \quad \mathrm{curl}\mathbf{E} = \mathbf{0}, \quad \mathrm{div}\mathbf{D} = 0, \tag{A3}$$

if the electric field is assumed to be quasi-static. For a material body in vacuum, all these physical quantities at the boundary ∂B_t, if in absence of surface charges, are required to satisfy

$$\tau\mathbf{n} = \mathbf{t}_a + \tau^*\mathbf{n}, (\mathbf{E} - \mathbf{E}^*) \times \mathbf{n} = \mathbf{0}, (\mathbf{D} - \mathbf{D}^*) \cdot \mathbf{n} = 0, \tag{A4}$$

where $\mathbf{t}_a$ is the applied mechanical traction per unit area of ∂B_t, $\tau^* = \varepsilon_0[\mathbf{E}^* \otimes \mathbf{E}^* - \frac{1}{2}(\mathbf{E}^* \cdot \mathbf{E}^*)\mathbf{I}]$ is the Maxwell stress, $\mathbf{E}*$ and $\mathbf{D}*$ are respectively the electric field vector and electric displacement vector of the electric field in vacuum, and $\varepsilon_0 = 8.85\,\mathrm{pF}/m$ is the permittivity of vacuum. $\mathbf{E}*$ and $\mathbf{D}*$ are connected by $\mathbf{D}^* = \varepsilon_0\mathbf{E}^*$ and

satisfy

$$\mathrm{curl}\mathbf{E}^* = \mathbf{0}, \quad \mathrm{div}\mathbf{D}^* = 0. \tag{A5}$$

A.2. Incremental field theory

If a perturbation $\dot{\mathbf{x}}(\mathbf{X}, t)$ along with an increment in the electric displacement $\dot{\mathbf{D}}_l$ is superimposed upon the static finite deformation, the incremental displacement may be expressed as $\mathbf{u} = \dot{\mathbf{x}}$, where the overdot denotes incremental quantities. According to the incremental field theory (Dorfmann and Ogden, 2006; Ogden, 2009), the linear incremental constitutive equations for incompressible isotropic electroactive materials are

$$\dot{\mathbf{T}}_0 = \mathbf{A_0}\mathbf{H} + \mathbf{\Gamma}_0\dot{\mathbf{D}}_{l0} + p\mathbf{H} - \dot{p}\mathbf{I}, \quad \dot{\mathbf{E}}_{l0} = \mathbf{\Gamma}_0^T\mathbf{H} + \mathbf{K}_0\dot{\mathbf{D}}_{l0}, \tag{A6}$$

where $\dot{\mathbf{T}}_0 = \mathbf{F}\dot{\mathbf{T}}$, $\dot{\mathbf{E}}_{l0} = \mathbf{F}^{-\mathrm{T}}\dot{\mathbf{E}}_l$, $\dot{\mathbf{D}}_{l0} = \mathbf{F}\dot{\mathbf{D}}_l$ are the 'push forward' versions of $\dot{\mathbf{T}}$, $\dot{\mathbf{E}}_l$, $\dot{\mathbf{D}}_l$ respectively, and $\mathbf{H} = \mathrm{grad}\,\mathbf{u}$ is the displacement gradient. $\mathbf{A}_0$, $\mathbf{\Gamma}_0$, and $\mathbf{K}_0$ are the effective electroelastic moduli tensors, whose Eulerian expressions are given by

$$A_{0piqj} = A_{0qjpi} = F_{p\alpha}F_{q\beta}\frac{\partial^2 W}{\partial F_{i\alpha}\partial F_{j\beta}}, \Gamma_{0piq} = \Gamma_{0ipq} = F_{p\alpha}F^{-1}_{\beta q}\frac{\partial^2 W}{\partial F_{i\alpha}\partial D_{l\beta}},$$
$$K_{0ij} = K_{0ji} = F^{-1}_{\alpha i}F^{-1}_{\beta j}\frac{\partial^2 W}{\partial D_{l\alpha}\partial D_{l\beta}}. \tag{A7}$$

For incompressible materials, the incremental motion is also subjected to the following incompressibility constraint

$$\mathrm{div}\,\mathbf{u} = \mathrm{tr}\,\mathbf{H} = 0. \tag{A8}$$

The incremental forms of the governing equations (A3) are

$$\mathrm{div}\dot{\mathbf{T}}_0 = \mathbf{0}, \quad \mathrm{curl}\dot{\mathbf{E}}_{l0} = \mathbf{0}, \quad \mathrm{div}\dot{\mathbf{D}}_{l0} = 0. \tag{A9}$$

Accordingly, the incremental form of boundary conditions for a material body in vacuum are

$$\left(\dot{\mathbf{E}}_{l0} - \dot{\mathbf{E}}^* - \mathbf{H}^{\mathrm{T}}\mathbf{E}^*\right) \times \mathbf{n} = \mathbf{0}, \left(\dot{\mathbf{D}}_{l0} + \mathbf{H}\mathbf{D}^* - \dot{\mathbf{D}}^*\right) \cdot \mathbf{n} = 0, \tag{A10}$$

$$\dot{\mathbf{T}}_0^{\mathrm{T}}\mathbf{n} = \dot{\mathbf{t}}_{A0} + \dot{\tau}^*\mathbf{n} - \boldsymbol{\tau}^*\mathbf{H}^{\mathrm{T}}\mathbf{n}, \tag{A11}$$

where $\dot{\mathbf{t}}_{A0}\mathrm{d}a = \dot{\mathbf{t}}_A\mathrm{d}A$, with $\mathbf{t}_A$ being the applied mechanical traction per unit area of ∂B_r, $\mathrm{d}a$ and $\mathrm{d}A$ are respectively the infinitesimal area elements in the deformed and reference configurations. Here, the incremental fields $\dot{\mathbf{E}}^*$ and $\dot{\mathbf{D}}^*$ are related by $\dot{\mathbf{D}}^* = \varepsilon_0\dot{\mathbf{E}}^*$ and satisfy

$$\mathrm{curl}\dot{\mathbf{E}}^* = \mathbf{0}, \quad \mathrm{div}\dot{\mathbf{D}}^* = 0. \tag{A12}$$

The incremental form of the Maxwell stress $\dot{\tau}^*$ in Eq. (A11) is given by

$$\dot{\tau}^* = \varepsilon_0\left[\dot{\mathbf{E}}^* \otimes \mathbf{E}^* + \mathbf{E}^* \otimes \dot{\mathbf{E}}^* - \left(\mathbf{E}^* \cdot \dot{\mathbf{E}}^*\right)\mathbf{I}\right], \tag{A13}$$

and it is easy to show that $\mathrm{div}\dot{\boldsymbol{\tau}}^* = \mathbf{0}$.

Appendix B. Components of the effective electroelastic moduli tensors

According to Dorfmann and Ogden's theory (Dorfmann and Ogden, 2010), the following non-zero components of the effective electroelastic moduli tensors can be derived for the specified pre-deformation state:

$$\begin{aligned}
A_{01111} &= 2\lambda^2\left\{2W_{22}\left(1+\lambda^{-3}\right)^2+\lambda^{-1}\left[4W_{12}\lambda^{-1}+W_1\lambda^{-2}+2W_{11}\lambda^{-2}\right.\right.\\
&\quad\left.\left.+4W_{12}\lambda^{-4}+W_2\left(1+\lambda^{-3}\right)\right]\right\},\\
A_{01122} &= 8W_{12}\left(1+\lambda^{-3}\right)+4\lambda^2\left[(W_{11}+W_2)\lambda^{-4}+W_{22}\left(1+\lambda^{-3}\right)^2\right],\\
A_{01133} &= 2\lambda^3\left\{W_{12}\left(2+6\lambda^{-3}\right)+2\lambda^{-1}\left[(W_{11}+W_2)\lambda^{-1}\right.\right.\\
&\quad\left.\left.+2W_{22}\left(1+\lambda^{-3}\right)\right]+2D_z^2\left[2W_{26}\left(1+\lambda^{-3}\right)\right.\right.\\
&\quad\left.\left.+\lambda^{-2}\left(2W_{16}+W_{25}+W_{15}\lambda^{-2}+W_{25}\lambda^{-3}\right)\right]\right\},\\
A_{03333} &= 2\lambda^4\left\{2W_{11}+8W_{12}\lambda^{-1}+W_1\lambda^{-2}+8W_{22}\lambda^{-2}\right.\\
&\quad+2W_2\lambda^{-3}+2D_z^4\left(4W_{66}+4W_{56}\lambda^{-2}+W_{55}\lambda^{-4}\right)\\
&\quad+D_z^2\left[8W_{16}+16W_{26}\lambda^{-1}+\lambda^{-2}(4W_{15}+6W_6\right.\\
&\quad\left.\left.\left.+8W_{25}\lambda^{-1}+W_5\lambda^{-2}\right)\right]\right\},\\
A_{01313} &= 2\lambda^{-1}\left(W_1+D_z^2W_6+W_2\lambda^{-1}\right), A_{01331} = -2\lambda W_2+2D_z^2W_6\lambda^{-1},\\
A_{03131} &= 2\lambda^2\left\{W_1+W_2\lambda^{-1}+D_z^2\left[W_5\lambda^{-2}+W_6\left(2+\lambda^{-3}\right)\right]\right\},\\
A_{01212} &= 2\lambda\left(W_2+W_1\lambda^{-2}\right), A_{01221} = -2W_2\lambda^{-2},\\
\Gamma_{0113} &= 4D_z\lambda^3\left\{W_{26}\left(1+\lambda^{-3}\right)+\lambda^{-2}\left[W_{16}+W_{25}\left(1+\lambda^{-3}\right)\right.\right.\\
&\quad\left.\left.+\lambda^{-2}\left(W_{15}+W_{24}+W_{14}\lambda^{-2}+W_{24}\lambda^{-3}\right)\right]\right\},\\
\Gamma_{0131} &= 2D_z\lambda^2\left(W_6+W_5\lambda^{-2}+W_6\lambda^{-3}\right),\\
\Gamma_{0333} &= 4D_z\lambda^4\left\{W_{16}+D_z^2\left[2W_{66}+3W_{56}\lambda^{-2}\right.\right.\\
&\quad\left.+\lambda^{-4}\left(2W_{46}+W_{55}+W_{45}\lambda^{-2}\right)\right]\\
&\quad+\lambda^{-1}\left[2W_{26}+\lambda^{-1}\left(W_{15}+2W_6+2W_{25}\lambda^{-1}\right.\right.\\
&\quad\left.\left.\left.+W_{14}\lambda^{-2}+W_5\lambda^{-2}+2W_{24}\lambda^{-3}\right)\right]\right\},\\
K_{011} &= 2\lambda\left(W_4+W_5\lambda^{-1}+W_6\lambda^{-2}\right),\\
K_{033} &= 2\lambda^4\left\{\lambda^{-2}\left(W_6+W_5\lambda^{-2}+W_4\lambda^{-4}\right)\right.\\
&\quad+2D_z^2\left[W_{66}+2W_{56}\lambda^{-2}\right.\\
&\quad\left.\left.+\lambda^{-4}\left(2W_{46}+W_{55}+2W_{45}\lambda^{-2}+W_{44}\lambda^{-4}\right)\right]\right\},
\end{aligned}$$

where $W_{ij} = \partial^2 W/\partial I_i \partial I_j$.

Appendix C. Elements of d_{ij}

$$\begin{aligned}
d_{14} &= \left(c_{11}+\mu\lambda^{-1}\right)\left[\frac{n}{r_o}J'_n(\eta_4 r_o)-\frac{n}{r_o^2}J_n(\eta_4 r_o)\right]\\
&\quad+c_{12}\frac{1}{r_o}\left[-\eta J'_n(\eta_4 r_o)+\frac{n}{r_o}J_n(\eta_4 r_o)\right],\\
d_{18} &= \left(c_{11}+\mu\lambda^{-1}\right)\left[\frac{n}{r_o}Y'_n(\eta_4 r_o)-\frac{n}{r_o^2}Y_n(\eta_4 r_o)\right]\\
&\quad+c_{12}\frac{1}{r_o}\left[-nY'_n(\eta_4 r_o)+\frac{n}{r_o}Y_n(\eta_4 r_o)\right],\\
d_{1j} &= -\left(c_{11}+\mu\lambda^{-1}\right)Z''_n\left(\eta_j r_o\right)+c_{12}\frac{1}{r_o}\left[\frac{n^2}{r_o}Z_n\left(\eta_j r_o\right)-Z'_n\left(\eta_j r_o\right)\right]\\
&\quad+\left(c_{13}k\zeta_{1j}+e_{31}k\zeta_{2j}-\zeta_{3j}\right)Z_n\left(\eta_j r_o\right),\\
d_{24} &= -c_{661}J''_n(\eta_4 r_o)-\left(c_{662}+\mu\lambda^{-1}\right)\frac{1}{r_o}\left[\frac{n^2}{r_o}J_n(\eta_4 r_o)-J'_n(\eta_4 r_o)\right],\\
d_{28} &= -c_{661}Y''_n(\eta_4 r_o)-\left(c_{662}+\mu\lambda^{-1}\right)\frac{1}{r_o}\left[\frac{n^2}{r_o}Y_n(\eta_4 r_o)-Y'_n(\eta_4 r_o)\right],\\
d_{2j} &= c_{661}\left[\frac{n}{r_o}Z'_n\left(\eta_j r_o\right)-\frac{n}{r_o^2}Z_n\left(\eta_j r_o\right)\right]\\
&\quad-\left(c_{662}+\mu\lambda^{-1}\right)\frac{1}{r_o}\left[-nZ'_n\left(\eta_j r_o\right)+\frac{n}{r_o}Z_n\left(\eta_j r_o\right)\right],\\
d_{34} &= -\left(c_{551}+\mu\lambda^{-1}-\frac{4\beta^2}{\varepsilon_0}D_z^2\right)k\frac{n}{r_o}J_n(\eta_4 r_o),\\
d_{38} &= -\left(c_{551}+\mu\lambda^{-1}-\frac{4\beta^2}{\varepsilon_0}D_z^2\right)k\frac{n}{r_o}Y_n(\eta_4 r_o),
\end{aligned}$$

Please cite this article as: Y. Su et al., On buckling of a soft incompressible electroactive hollow cylinder, International Journal of Solids and Structures (2016), http://dx.doi.org/10.1016/j.ijsolstr.2016.07.008

$$d_{3j} = \left(c_{551} + \mu\lambda^{-1} - \frac{4\beta^2}{\varepsilon_0}D_z^2\right)kZ'_n(\eta_j r_o) + c_{552}\zeta_{1j}Z'_n(\eta_j r_o) + e_{15}\zeta_{2j}Z'_n(\eta_j r_o),$$

$$d_{44} = 0, d_{48} = 0,$$

$$d_{4j} = \frac{n}{r_o}\zeta_{2j}Z_n(\eta_j r_o) + \frac{n}{r_o}\frac{D_z}{\varepsilon}\zeta_{1j}Z_n(\eta_j r_o),$$

$$d_{54} = -k\left(e_{15} + \frac{\varepsilon_0}{\varepsilon}D_z\right)\frac{n}{r_o}J_n(\eta_4 r_o),$$

$$d_{58} = -k\left(e_{15} + \frac{\varepsilon_0}{\varepsilon}D_z\right)\frac{n}{r_o}Y_n(\eta_4 r_o),$$

$$d_{5j} = \left(e_{15} + \frac{\varepsilon_0}{\varepsilon}D_z\right)kZ'_n(\eta_j r_o) + e_{15}\zeta_{1j}Z'_n(\eta_j r_o) - \varepsilon_{11}\zeta_{2j}Z'_n(\eta_j r_o),$$

$$d_{19} = -\varepsilon_0\frac{D_z}{\varepsilon}kK_n(kr_o), d_{29} = 0,$$

$$d_{39} = \varepsilon_0\frac{D_z}{\varepsilon}K'_n(kr_o), d_{49} = -\frac{1}{r_o}nK_n(kr_o), d_{59} = \varepsilon_0 K'_n(kr_o),$$

$$d_{64} = \left(c_{11} + \mu\lambda^{-1}\right)\left[\frac{n}{r_i}J'_n(\eta_4 r_i) - \frac{n}{r_i^2}J_n(\eta_4 r_i)\right] + c_{12}\frac{1}{r_i}\left[-nJ'_n(\eta_4 r_i) + \frac{n}{r_i}J_n(\eta_4 r_i)\right],$$

$$d_{68} = \left(c_{11} + \mu\lambda^{-1}\right)\left[\frac{n}{r_i}Y'_n(\eta_4 r_i) - \frac{n}{r_i^2}Y_n(\eta_4 r_i)\right] + c_{12}\frac{1}{r_i}\left[-nY'_n(\eta_4 r_i) + \frac{n}{r_i}Y_n(\eta_4 r_i)\right],$$

$$d_{6j} = -\left(c_{11} + \mu\lambda^{-1}\right)Z''_n(\eta_j r_i) + c_{12}\frac{1}{r_i}\left[\frac{n^2}{r_i}Z_n(\eta_j r_i) - Z'_n(\eta_j r_i)\right] + (c_{13}k\zeta_{1i} + e_{31}k\zeta_{2i} - \zeta_{3i})Z_n(\eta_j r_i),$$

$$d_{74} = -c_{661}J''_n(\eta_4 r_i) - \left(c_{662} + \mu\lambda^{-1}\right)\frac{1}{r_i}\left[\frac{n^2}{r_i}J_n(\eta_4 r_i) - J'_n(\eta_4 r_i)\right],$$

$$d_{78} = -c_{661}Y''_n(\eta_4 r_i) - \left(c_{662} + \mu\lambda^{-1}\right)\frac{1}{r_i}\left[\frac{n^2}{r_i}Y_n(\eta_4 r_i) - Y'_n(\eta_4 r_i)\right],$$

$$d_{7j} = c_{661}\left[\frac{n}{r_i}Z'_n(\eta_j r_i) - \frac{n}{r_i^2}Z_n(\eta_j r_i)\right] - \left(c_{662} + \mu\lambda^{-1}\right)\frac{1}{r_i}\left[-nZ'_n(\eta_j r_i) + \frac{n}{r_i}Z_n(\eta_j r_i)\right],$$

$$d_{84} = -\left(c_{551} + \mu\lambda^{-1} - \frac{4\beta^2}{\varepsilon_0}D_z^2\right)k\frac{n}{r_i}J_n(\eta_4 r_i),$$

$$d_{88} = -\left(c_{551} + \mu\lambda^{-1} - \frac{4\beta^2}{\varepsilon_0}D_z^2\right)k\frac{n}{r_i}Y_n(\eta_4 r_i),$$

$$d_{8j} = \left(c_{551} + \mu\lambda^{-1} - \frac{4\beta^2}{\varepsilon_0}D_z^2\right)kZ'_n(\eta_j r_i) + c_{552}\zeta_{1i}Z'_n(\eta_j r_i) + e_{15}\zeta_{2i}Z'_n(\eta_j r_i),$$

$$d_{94} = 0, d_{98} = 0,$$

$$d_{9j} = \frac{n}{r_i}\zeta_{2i}Z_n(\eta_j r_i) + \frac{n}{r_i}\frac{D_z}{\varepsilon}\zeta_{1i}Z_n(\eta_j r_i),$$

$$d_{101} = -k\left(e_{15} + \frac{\varepsilon_0}{\varepsilon}D_z\right)\frac{n}{r_i}J_n(\eta_4 r_i),$$

$$d_{105} = -k\left(e_{15} + \frac{\varepsilon_0}{\varepsilon}D_z\right)\frac{n}{r_i}Y_n(\eta_4 r_i),$$

$$d_{10i} = \left(e_{15} + \frac{\varepsilon_0}{\varepsilon}D_z\right)kZ'_n(\eta_j r_i) + e_{15}\zeta_{1i}Z'_n(\eta_j r_i) - \varepsilon_{11}\zeta_{2i}Z'_n(\eta_j r_i),$$

$$d_{610} = -\varepsilon_0\frac{D_z}{\varepsilon}kI_n(kr_i), d_{710} = 0,$$

$$d_{810} = \varepsilon_0\frac{D_z}{\varepsilon}I'_n(kr_i),$$

$$d_{910} = -\frac{n}{r_i}I_n(kr_i), d_{1010} = \varepsilon_0 I'_n(kr_i),$$

where, $j = 1, 2, 3, 5, 6, 7$, for $j = 1, 2, 3$, $Z(\cdot) = J(\cdot)$, for $j = 5, 6, 7$, $Z(\cdot) = Y(\cdot)$; and the notations $\eta_{j+4} = \eta_j$ and $\zeta_{n(j+4)} = \zeta_{nj}$ $(j, n = 1, 2, 3)$ have been adopted.

References

Bertoldi, K., Gei, M., 2011. Instabilities in multilayered soft dielectrics. J. Mech. Phys. Solids 59 (1), 18–42.

Bhattacharya, K., Li, J., Xiao, Y., 2004. Electromechanical models for optimal design and effective behavior of electroactive polymers. In: Bar-Cohen, Y. (Ed.), Electroactive Polymer (EAP) Actuators as Artificial Muscles: Reality, Potential and Challenges. SPIE Press, Bellingham, WA, pp. 363–384.

Biot, M.A., 1963. Exact theory of buckling of a thick slab. Appl. Sci. Res. 12 (2), 183–198.

Blok, J., LeGrand, D.G., 1969. Dielectric breakdown of polymer films. J. Appl. Phys. 40 (1), 288–293.

Cameron, C.G., Szabo, J.P, Johnstone, S., et al., 2008. Linear actuation in coextruded dielectric elastomer tubes. Sens. Actuators A Phys. 147 (1), 286–291.

Carpi, F., De Rossi, D., 2004. Dielectric elastomer cylindrical actuators: electromechanical modelling and experimental evaluation. Mater. Sci. Eng. C Mater. Biol. Appl. 24 (4), 555–562.

Chen, C.L., 1973. On the electroacoustic waves guided by a cylindrical piezoelectric interface. J. Appl. Phys. 44 (9), 3841–3847.

Chen, W.Q., Dai, H.H., 2012. Waves in pre-stretched incompressible soft electroactive cylinders: exact solution. Acta Mech. Solida Sin. 25 (5), 530–541.

deBotton, G., Tevet-Deree, L., Socolsky, E.A., 2007. Electroactive heterogeneous polymers: analysis and applications to laminated composites. Mech. Adv. Mater. Struct. 14 (1), 13–22.

Díaz-Calleja, R., Sanchis, M.J., Riande, E., 2009. Effect of an electric field on the bifurcation of a biaxially stretched incompressible slab rubber. Eur. Phys. J. E 30 (4), 417–426.

Dıaz-Calleja, R., Sanchis, M.J., Riande, E., 2010. Instability of incompressible cylinder rubber tubes under radial electric fields. Eur. Phys. J. E 32 (2), 183–190.

Ding, H.J., Chen, W.Q., 2001. Three Dimensional Problems of Piezoelasticity. Nova Science Publishers, New York.

Ding, H.J., Chen, W.Q., Zhang, L.C., 2006. Elasticity of Transversely Isotropic Materials. Springer, Dordrecht.

Dorfmann, A., Haughton, D.M., 2006. Stability and bifurcation of compressed elastic cylindrical tubes. Int. J. Eng. Sci. 44 (18), 1353–1365.

Dorfmann, A., Ogden, R.W., 2006. Nonlinear electroelastic deformations. J. Elast. 82 (2), 99–127.

Dorfmann, A., Ogden, R.W., 2010. Nonlinear electroelastostatics: incremental equations and stability. Int. J. Eng. Sci. 48 (1), 1–14.

Dorfmann, L., Ogden, R.W., 2014. Instabilities of an electroelastic plate. Int. J. Eng. Sci. 77, 79–101.

Ericksen, J.L., 2007. Theory of elastic dielectrics revisited. Arch. Ration. Mech. Anal. 183 (2), 299–313.

Euler, L., Carathéodory, C., 1952. Methodus inveniendi lineas curvas maximi minimive proprietate gaudentes sive solutio problematis isoperimetrici latissimo sensu accepti. Springer Science & Business Media.

Goriely, A., Vandiver, R., Destrade, M., 2008. Nonlinear Euler buckling. Proc. R. Soc. Lond. Ser. A Math. Phys. Eng. Sci. 464 (2099), 3003–3019.

Huang, C., Zhang, Q.M., Bhattacharya, K., 2004. All-organic dielectric-percolative three-component composite materials with high electromechanical response. Appl. Phys. Lett. 84 (22), 4391–4393.

McMeeking, R.M., Landis, C.M., 2005. Electrostatic forces and stored energy for deformable dielectric materials. J. Appl. Mech. 72 (4), 581–590.

O'Halloran, A., O'Malley, F., McHugh, P.A., 2008. Review on dielectric elastomer actuators, technology, applications, and challenges. J. Appl. Phys. 104 (7), 071101.

Ogden, R.W., 2009. Incremental elastic motions superimposed on a finite deformation in the presence of an electromagnetic field. Int. J. Nonlinear Mech. 44 (5), 570–580.

Pan, F., Beatty, M.F., 1997. Remarks on the instability of an incompressible and isotropic hyperelastic, thick-walled cylindrical tube. J. Elast. 48 (3), 218–239.

Pelrine, R., Kornbluh, R., Joseph, J., et al., 2000. High-field deformation of elastomeric dielectrics for actuators. Mater. Sci. Eng. C Mater. Biol. Appl. 11 (2), 89–100.

Pelrine, R.E., Kornbluh, R.D., Joseph, J.P., 1998. Electrostriction of polymer dielectrics with compliant electrodes as a means of actuation. Sens. Actuators A Phys. 64 (1), 77–85.

Plante, J.S., Dubowsky, S., 2006. Large-scale failure modes of dielectric elastomer actuators. Int. J. Solids Struct. 43 (25), 7727–7751.

Rudykh, S., deBotton, G., 2011. Stability of anisotropic electroactive polymers with application to layered media. Z. Angew. Math. Phys. 62 (6), 1131–1142.

Shmuel, G., Gei, M., deBotton, G., 2012. The Rayleigh–Lamb wave propagation in dielectric elastomer layers subjected to large deformations. Int. J. Nonlinear Mech. 47 (2), 307–316.

Stark, K.H., Garton, C.G., 1955. Electric strength of irradiated polythene. Nature 176, 1225–1226.

Please cite this article as: Y. Su et al., On buckling of a soft incompressible electroactive hollow cylinder, International Journal of Solids and Structures (2016), http://dx.doi.org/10.1016/j.ijsolstr.2016.07.008

Su, Y.P., Wang, H.M., Zhang, C.L., Chen, W.Q., 2016. Propagation of non-axisymmetric waves in an infinite soft electroactive hollow cylinder under uniform biasing fields. Int. J. Solids Struct. 81, 262–273.
Suo, Z., Zhao, X., Greene, W.H., 2008. A nonlinear field theory of deformable dielectrics. J. Mech. Phys. Solids 56 (2), 467–486.
Toupin, R.A., 1956. The elastic dielectric. J. Ration. Mech. Anal. 5 (6), 849–915.
Wilkes, E.W., 1955. On the stability of a circular tube under end thrust. Q. J. Mech. Appl. Math. 8 (1), 88–100.
Wissler, M., Mazza, E., 2007. Electromechanical coupling in dielectric elastomer actuators. Sens. Actuators A Phys. 138 (2), 384–393.
Zhang, C., Chen, H., Liu, L., et al., 2015. Modelling and characterization of inflated dielectric elastomer actuators with tubular configuration. J. Phys. D Appl. Phys. 48 (24), 245502.
Zhao, X., Hong, W., Suo, Z., 2007. Electromechanical hysteresis and coexistent states in dielectric elastomers. Phys. Rev. B. 76 (13), 134113.
Zhao, X., Suo, Z., 2007. Method to analyze electromechanical stability of dielectric elastomers. Appl. Phys. Lett. 91 (6), 061921.
Zhao, X., Suo, Z., 2008. Electrostriction in elastic dielectrics undergoing large deformation. J. Appl. Phys. 104 (12), 123530.
Zhou, J., Jiang, L., Khayat, R.E., 2014. Electromechanical response and failure modes of a dielectric elastomer tube actuator with boundary constraints. Smart Mater. Struct. 23 (4), 045028.
Zhu, J., Stoyanov, H., Kofod, G., et al., 2010. Large deformation and electromechanical instability of a dielectric elastomer tube actuator. J. Appl. Phys. 108 (7), 074113.

Please cite this article as: Y. Su et al., On buckling of a soft incompressible electroactive hollow cylinder, International Journal of Solids and Structures (2016), http://dx.doi.org/10.1016/j.ijsolstr.2016.07.008